Diplomarbeit

Distribution of Serotonin Reuptake Transporters in the Human Brain Comparing PET and Post Mortem Data

zur Erlangung des akademischen Grades

Doktor der gesamten Heilkunde (Dr. med. univ.)

an der

Medizinischen Universität Wien (MUW)

ausgeführt an der

Klinischen Abteilung für Biologische Psychiatrie,

Universitätsklinik für Psychiatrie und Psychotherapie

unter der Anleitung von

Assoc. Prof. Rupert Lanzenberger, MD PD
Dr. techn. Markus Savli, MSc

eingereicht von

Gregor GRYGLEWSKI

Matr. Nr.: 0942164

Ort, Datum   Unterschrift

_____   _____

0 ACKNOWLEDGEMENTS

1 CONTENTS

2 ABSTRACT

Background

Alterations of the serotonin neuromodulatory system have been shown in many psychiatric disorders. The serotonin reuptake transporter (SERT) is responsible for the uptake of serotonin from the extracellular fluid and thus for the termination of neurotransmission mediated by this monoamine. Therefore, SERT has been the target of a vast amount of psychiatric and illicit drugs. Up-to-date topologically comparative *in vivo* quantification of SERT using positron emission tomography (PET) in the human brain is sparse. The effects of age and sex on regional SERT expression need to be clarified. The comparison of binding potentials (BP) and binding density (B_{max}) *post mortem* allows approximation of absolute transporter availability *in vivo*.

Methods

30 healthy subjects (11 women) aged 31.1 (SD 10.0) years were measured with PET using the radioligand [^{11}C]DASB. BP_{ND} maps of SERT for each Brodmann and Automated Anatomical Labelling region of interest (ROI) were computed. T-tests were performed comparing ROI binding potentials between sexes. Correlation coefficients were calculated between ROI BP and age. Mean ROI BPs and *post mortem* transporter densities were correlated for various autoradiography studies included in the analyses. Lastly, linear equations connecting BP to absolute SERT density, B_{max} (pmol/g tissue), were generated using age-corrected values.

Results

Highest SERT BPs were observed in brainstem ROIs, particularly the raphe nuclei. No significant effects of sex or age on BP were assessed. Binding potentials were highly correlated with B_{max} data from 8 out of 10 *post mortem* studies (Pearson's r: $0.82 - 0.95$; p-values: $0.02 - 10^{-9}$). Seven linear equations (R^2: $0.53 - 0.91$) to calculate SERT B_{max} using BP_{ND} were obtained. The most significant equation ($R^2 = 0.91$; $p < 10^{-11}$) is $[^3H]Cyanoimipramine\ binding = 1.1 + 18.9 * [^{11}C]DASB\ BP_{ND}$.

Discussion & Relevance

The high agreement between *post mortem* SERT density and BP_{ND} further validates quantification of SERT with PET and the highly selective tracer [^{11}C]DASB in subcortical, as well as in cortical brain regions. The calculation of B_{max} using PET BP allows comparison of brain protein concentrations *in vivo* independent of tracer used. This is an essential prerequisite for the development of integrated models in multimodal neuroimaging which might predict local changes in brain activation elicited by psychiatric medication measured with pharmacological functional magnetic resonance imaging based on multi-receptor molecular imaging *in vivo* with PET. However, to increase the precision of this approach, further studies with alignment of *in vivo* and *post mortem* coordinates are necessary.

3 ZUSAMMENFASSUNG

Hintergrund

Veränderungen des serotonergen Systems wurden bei vielen psychiatrischen Erkrankungen aufgedeckt. Der Serotonin Wiederaufnahme Transporter (SERT), als Angriffspunkt zahlreicher Psychopharmaka, ist für die Aufnahme von Serotonin aus dem Extrazellularraum und damit für die Beendigung der Neurotransmission durch dieses Monoamin verantwortlich. Bisher wurden kaum topologisch vergleichende Daten zur Quantifizierung von SERT mittels Positronen-Emissions-Tomographie (PET) *in vivo* veröffentlicht. Ebenso ist der Einfluss von Geschlecht und Alter auf die SERT Expression nicht zur Gänze geklärt. Der Vergleich von maximaler Bindungsdichte (B_{max}) *post mortem* und PET Bindungspotentialen (BP) bietet eine Möglichkeit absolute SERT Dichten in verschiedenen Hirnregionen *in vivo* zu schätzen.

Methoden

30 gesunde Probanden (11 Frauen), mittleres Alter 31,1 (SD 10,0) Jahre wurden jeweils einer PET Messung mit dem Tracer [^{11}C]DASB unterzogen. BP_{ND} Werte von SERT für jede Brodmann und Automated Anatomical Labeling region of interest (ROI) wurden ermittelt. Die ROI BP Werte der Geschlechter wurden anhand von T-tests verglichen. Alter und ROI BP wurden korreliert. ROI BP Mittelwerte und publizierte B_{max} Werte wurden für jede untersuchte *post mortem* Studie separat verglichen. Abschließend wurden anhand alterskorrigierter Daten lineare Modelle erstellt, um SERT B_{max} (pmol/g Gewebe) aus BP berechnen zu können.

Ergebnisse

Höchste SERT BP wurden in Hirnstammregionen, insbesondere in den Raphe Kernen, erhoben. Kein signifikanter Einfluss von Geschlecht oder Alter auf BP wurde festgestellt. BP und B_{max} aus 8 von 10 untersuchten Studien waren hoch korreliert (Pearsons r: $0,82 - 0,95$; p: $0,02 - 10^{-9}$). 7 lineare Modelle (R^2: $0,53 - 0,91$) für die Berechnung von SERT B_{max} anhand von BP_{ND} wurden erstellt. Die signifikanteste Gleichung ($R^2 = 0,91$; $p < 10^{-11}$) ist $[^3H]Cyanoimipramine\ binding = 1,1 + 18,9 * [^{11}C]DASB\ BP_{ND}$.

Diskussion & Relevanz

Die hohe Übereinstimmung von BP und *post mortem* erhobenen SERT Dichten, bestätigt die Validität der Quantifizierung von SERT mittels PET und dem hochselektiven Tracer [^{11}C]DASB auch in kortikalen Hirnregionen. Die Berechnung von B_{max} aus PET BP erlaubt den Vergleich verschiedener Proteinkonzentrationen *in vivo* unabhängig vom verwendeten Tracer. Dadurch wird die Entwicklung integrierter Modelle im multimodalen Neuroimaging ermöglicht, mit denen regionale Veränderungen der Gehirnfunktion durch Psychopharmaka, die mittels funktionaler Magnetresonanztomographie dargestellt werden, anhand der molekularen Bildgebung mit PET vorhergesagt werden könnten. Um die Präzision dieser Methode zu erhöhen, sind jedoch Studien mit Abstimmung von *post mortem* und *in vivo* Koordinaten nötig.

4 BACKGROUND

4.1 Investigating Brain Receptor and Transporter Systems

4.1.1 PET

PET molecular imaging is based on the application of tracers labelled with a nuclide prone to β+ decay. The resultantly emitted positrons (e^+) are decelerated in the surrounding tissue until they interact with electrons (e^-) and together transform into high-energy photons (γ-radiation) moving in opposite (~180°) directions, a process called annihilation. Two photons arising from one such interaction can reach two opposite scintillation detectors and produce a current that is amplified at approximately the same time, a coincident event occurs. The straight line connecting two detectors which registered the same annihilation event is called line of response (LOR). During a PET scan many such LORs are acquired yielding a sinogram, which after reconstruction via back projections results in tomographic images showing the distribution of radioactivity in the imaged volume. This distribution in turn is dependent on the characteristics of the tracer molecules. These are designed to bind certain biological structures, e.g. receptors or transporter molecules, or to mimic other substances as e.g. ^{18}Fluordesoxyglucose to visualize metabolic or kinetic physiological processes (Heiss & Herholz 2006).

4.1.1.1 Tracers

Imaging of human brain receptors *in vivo* requires tracers with suitable chemical characteristics: High specificity, high affinity for the respective receptor, low toxicity, stable labelling, quick uptake and distribution in brain tissue, and few, rapidly cleared, and preferably unlabelled metabolites (Heiss & Herholz 2006, Kung 1991). Obviously, when choosing the right tracer, certain trade-offs have to be made, as some of the properties are mutually counteracting. For example, with lipophilicity both, tissue penetration and non-specific binding, increase, which excludes many common antidepressants as practicable tracers for the serotonin transporter *in vivo*.

So far, of all the possible molecules capable of binding to SERT only the following were selected for long range human investigations with PET (Saulin et al 2012):

4.1.1.1.1 [^{11}C]McN5652

In the late 1980s, the ability of McN5652 to potently inhibit serotonin uptake was discovered by Shank et al (1988). A few years later, the [^{11}C]labelled (+)enantiomer of McN5652, [^{11}C](+)McN5652 was suggested for PET imaging and found to be superior to the (−)enantiomer in terms of specific binding to SERT in mice (Suehiro et al 1993). Thereafter, quantification of SERT in humans was successfully performed with [^{11}C]McN5652. Reliable results, however, were restricted to regions with high transporter densities (Parsey et al 2000). Therefore [^{11}C]McN5652 was soon replaced by tracers with lower non-specific binding.

4.1.1.1.2 [^{11}C]DASB

Wilson and Houle (1999) were the first to synthesize [^{11}C]DASB and report of its over 1000-fold selectivity for SERT over the dopamine- and norepinephrine reuptake transporters (Wilson et al 2000). In the first human trials, [^{11}C]DASB accumulated in SERT rich regions and was displaced by SSRIs (selective serotonin reuptake inhibitors), which confirmed its suitability for the imaging of SERT (Houle et al 2000). Compared to [^{11}C]McN5652 [^{11}C]DASB showed lower non-specific binding and faster brain uptake, making it the first PET tracer to allow imaging of SERT in brain regions with low densities (Frankle et al 2004). Furthermore, measurement of *in vivo* SERT occupancy by drugs such as SSRIs became possible with [^{11}C]DASB and PET.

4.1.1.1.3 [^{11}C]MADAM

Chalon et al (2003) proposed [^{11}C]MADAM as a suitable tracer for PET imaging of the SERT due to its high selectivity and low non-specific binding in *post mortem* rat and human brains. The success of the ligand at visualizing SERT distribution in the first *in vivo* experiments with [^{3}H]labelled MADAM in mice(Larsen et al 2004), followed by the first [^{11}C]MADAM PET scans of monkey brains (Halldin et al 2005), prompted the application in human PET studies (Lundberg et al 2005). Nowadays [^{11}C]MADAM is continuously used as a reliable tracer for imaging of SERT with PET (Lundberg et al 2006).

4.1.1.2 Binding Potential

The following is a digest of information on the definition and calculation of binding potential commonly used by many authors. The nomenclature used here was faithfully adapted from a detailed review on the topic by Innis et al (2007).

In many PET studies the term "binding potential" (BP) is the main parameter used to answer the issues at hand. It was introduced by Mintun et al (1984) as the ratio of absolute density of a targeted molecular structure (B_{max}) and the dissociation constant (K_D) of the ligand at its target.

$$BP = \frac{B_{max}}{K_D} = B_{max} * affinity \tag{1}$$

The dissociation constant (K_D) is the multiplicative inverse of the affinity of the tracer to its target and is defined as the concentration of free ligand (F) necessary to occupy 50% of the binding sites of the target at equilibrium.

$$K_D = \frac{1}{affinity} = \frac{k_{OFF}}{k_{ON}} = \frac{B_{avail} * F}{B} = \frac{(B_{max} - B) * F}{B} \tag{2}$$

Equation 2 is derived from equation 3. According to the law of mass action, the equilibrium is defined as a state in which the amount of free ligand associating with available target molecules (B_{avail}) equals the amount of ligand bound (B) dissociating from the target:

$$F * B_{avail} * k_{ON} = B * k_{OFF} \tag{3}$$

k_{ON} and k_{OFF} are the association and dissociation rate constants, respectively. Since B_{max} and K_D are not easily determined *in vivo*, for reasons later to be clarified, the BP is currently the best means to compare the relative abundance of the molecules visualized among different regions and subjects *in vivo*.

However, what would be of actual interest in many cases, is the absolute density of the targeted molecular structure (B_{max}) or the amount of target sites available for binding (B_{avail}), as a fraction (B) may be occupied by endogenous or exogenous ligands.

$$B_{avail} = B_{max} - B \tag{4}$$

But the information PET scanners can provide are the concentrations of radioactivity per units of volume (voxels), a measure which is regardless of whether the origin of the activity are tracer molecules specifically bound to their targets, free in tissue or bound to other structures. For the purpose of transforming this data into a comprehensible measure of available target molecules, the pharmacological equations mentioned above were fed with assumptions about the respective characteristics of molecular imaging to yield the concept of binding potentials. In detail, equation 2 can be rearranged to equation 5.

$$\frac{B}{F} = \frac{B_{max}}{K_D + F} \tag{5}$$

Given the low tracer doses applied in molecular imaging procedures, the concentration of free tracer (F) is far below K_D. Therefore, its contribution to the nominator on the right side of the equation is neglected, resulting in the formula defining the binding potential:

$$\frac{B}{F} = \frac{B_{max}}{K_D} = BP \tag{6}$$

Using this formula and the concentrations read out from PET scans, various forms of the BP can be calculated according to the model used and measures made. B is replaced by C_S, the concentration of specifically bound tracer, which is the difference of total tracer concentration (C_T) and free and non-specifically bound, also called the non-displaceable concentration (C_{ND}). The latter can be obtained from a region known to be devoid of the target, e.g. in the case of SERT the cerebellum (Kish et al 2005). F can be replaced by the concentration of free or total tracer in plasma, if such measures are available, to obtain BP_F and BP_P, respectively.

Since in the current investigation no blood samples were taken during PET scans, calculations of BP are based on the assumption that the free concentration of tracer is in the vicinity of the non-displaceable concentration (C_{ND}). This is justified with the low non-specific binding of [^{11}C]DASB. Therefore, the following formula corresponds to the BP calculated in the course of the current investigation:

$$BP_{ND} = \frac{C_T - C_{ND}}{C_{ND}} \tag{7}$$

4.1.1.3 Technical limitations

Apart from limited tracer availability and high procurement costs the major limitations of PET are spatial and temporal resolution.

Temporal resolution is low due to the limited amount of radiation that is emitted per unit of time necessitating long image acquisition time
 to capture coherent images.

Spatial resolution is restricted by the size of single detector units utilised in PET scanners. Smaller sizes would reduce sensitivity to incoming radiation, but there is room for technical improvement. Despite the technical aspects, there are physical laws limiting spatial resolution of PET imaging, the most obvious will be named here.

Depending on their original energy, positrons travel a certain distance through tissue before finding their annihilation

Figure 1:
Two physical properties of PET imaging are symbolically (angles and distances are grossly overestimated) rendered. The distance a positron travels before annihilation is termed the positron range and averages 1.1 mm in water for ^{11}C tracers. Noncollinearity denotes deviations of the angle between the resulting photons from 180°. Reproduced from Rahmim and Zaidi (2008).

partner. The original energy in turn depends on the β+ decaying isotope used. For most clinical PET imaging procedures (isotopes: ^{11}C, ^{13}N, ^{15}O, ^{18}F) the average linear distance positrons travel ranges from 0.6 to 2.9 millimetres (Jodal et al 2012), but can be shortened by applying strong magnetic fields as in magnetic resonance imaging (MRI) to bend the course of the positrons, resulting in shorter linear distances from the place of isotope decay to the point of particle annihilation.

The kinetic energy the particles possess at the moment of annihilation translates into deviation of the angle at which photons are emitted from 180°, an effect called noncollinearity. This adds uncertainty to the assumption that the annihilation responsible for a coincidence event recorded took place on a straight line between the respective two detectors (LOR). These physical properties fundamentally limit spatial resolution of clinical PET imaging to 1.8 millimetres full-width-at-half-maximum (FWHM), while most scanners currently operate around 4 mm FWHM (Moses 2011).

Factors adding noise to the imaging process are the scatter of radiation and random coincidences originating from different annihilation events at approximately the same point in time (~10 nanoseconds) (Bailey 2005).

Given the spatial resolution of PET imaging procedures, analysis of small structures may suffer from so-called partial volume effects. If the extent of a ROI is smaller than twice the resolution FWHM, activity attributed to the voxels covering the ROI after reconstruction of the PET image is a blend of activities emitted by the structure of interest itself and surrounding tissue. Moreover, due to the positron range, borders between neighbouring structures are blurred in terms of activity. Thus, if a small structure accumulating high amounts of tracer is surrounded by non-active tissue, the resulting activity measures for respective voxels underestimate the activity of the small ROI, while overestimating the surround (Soret et al 2007).
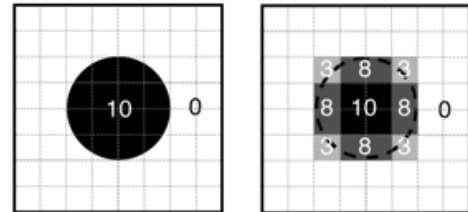
Figure 2:
Partial volume effect (PVE) for 2D pictures. The left tale shows a theoretical input to an imaging procedure with a resolution corresponding to the grid. The right tale shows the resulting image with grey values attributed to each pixel corresponding to the average grey value on the left side. Imagine a black ball the size of one pixel on a white carpet. The captured image could never do justice to its original darkness.
Reproduced from Soret et al (2007).

4.1.2 *POST MORTEM* STUDIES

Post mortem studies are the gold standard of topological quantification of molecular structures (Agam et al 2002) and constitute the fundament of *in vivo* molecular imaging. Each ligand applied in PET or SPECT (single-photon emission computed tomography) studies has been investigated *in vitro*, be it using cells expressing the recombinant target structure, or membranes or sections prepared from animals or humans. Thus, important characteristics of tracers are assessed before use in humans *in vivo*.
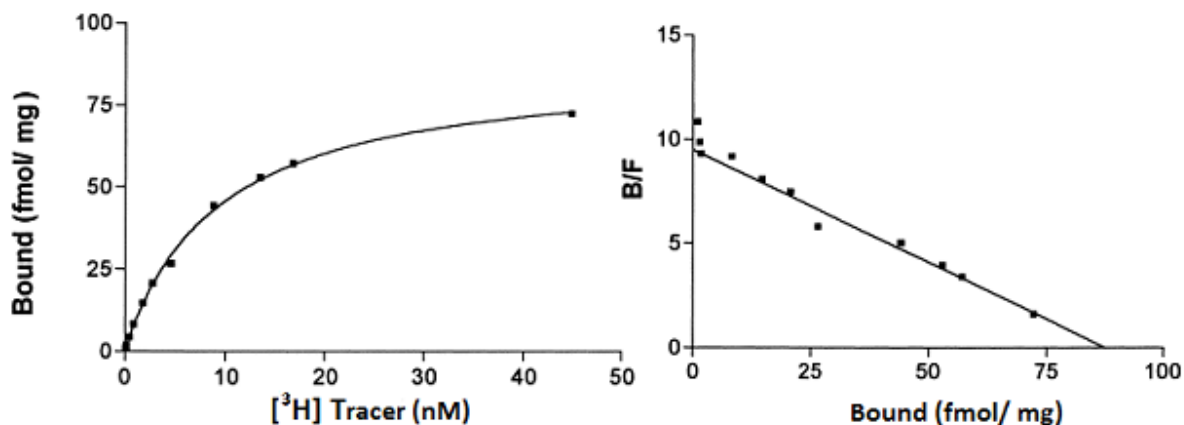
Figure 3:
Exemplary data of binding of a tracer to a receptor molecule at different concentrations (left). The resulting Scatchard plot is depicted on the right. The slope of the regression line equals affinity * -1
(B/F, ratio between ligand in the bound and ligand in the free compartement)
Reproduced from Castelli et al (2000).

One of the most crucial among these characteristics is the affinity of the tracer for its target, but also for other, similar structures as e.g. the dopamine- or norepinephrine transporters in the case of SERT tracers. One technique to quantify a tracer's affinity is to use different concentrations of radioactively labelled ligand in a binding assay and measure the amount of bound ligand at each concentration. Then, affinity can be obtained from the resulting data by applying Scatchard analysis (Scatchard 1949) or non-linear regression. To validate the tracer's specificity further, the distribution of its binding can be compared to the distribution of tracers known to bind the target structure reliably. Moreover, the tracer should be displaced by and only by other substances binding to the same target.

The advantages of *post mortem* studies are manifold. First of all, the investigator can determine the conditions of experiments arbitrarily: Temperature, pH, chemical properties of the buffer solution. There are no confounding factors to receptor quantification such as regional blood flow, metabolism, varying physiological substances competing for the target molecule, dynamic receptor conformation or sequestration. Lastly, in terms of resolution, autoradiography combined with electron microscopy can visualize subcellular compartments in great detail (Caro et al 1962).

The chief drawbacks of *post mortem* studies are sampling bias, limited information on subjects, degradation of tissue before experiments, unphysiological circumstances of binding and only cross-sectional study designs.

4.1.2.1 *Autoradiography*

Autoradiography is an imaging method capable of quantifying molecular structures in tissue sections at high resolution. For this purpose frozen brains are sectioned to an arbitrary thickness (10-100µm) using a cryotome and dried. Binding experiments are performed at a temperature above 4°C chosen by the experimenter. Sections are incubated in a buffer solution containing the tritiated specific ligand for approximately 60 to 90 minutes and consecutively washed for several minutes using buffer or water or both to displace unbound molecules. Given the slow dissociation rate of highly affine ligands, only a small fraction of bound ligands is released during washing. After drying, sections are apposed to tritium sensitive film for several days. The regional blackness of the film corresponds to the local radioactivity of the section it is exposed to which is subsequently calculated using tritiated standards as a reference.

In contrast to isotopes used in PET tracers ³H is prone to β− decay, that is, electron emission. These electrons, however, are low in energy (mean 6 keV, max. ~ 19 keV) and therefore easily absorbed (Berger et al 1964), showing a mean range ~ 3 µm in water (Prescott 1969), which makes autoradiography a safe method, but hinders a considerable amount of radiation from leaving the tissue under investigation itself. Therefore activity present in deeper levels of the section is underrepresented on the film. This effect was termed ³H- β-self-absorption and makes correction of measured activity necessary (Korr et al 1997), adding a source of variability to autoradiography data if tissue handling protocols are non-uniform.

The whole process is repeated with the addition of another specific ligand to the buffer solution to displace the tritiated tracer from the target. This allows the determination of non-specific binding which is subtracted from total binding to obtain specific binding.

If the concentration of ligand used is several orders higher than K_D, specific binding is approximately equal to total binding density. If the concentration chosen is not sufficient to bind most target sites available, B_{max} must be calculated with a transform of Equation 5.

Table 1 contains key methodical features for all published autoradiography studies investigating SERT in a neurologically and psychiatrically healthy group of subjects.

4.1.2.2 Membrane Binding Studies

Membrane binding studies are similar to autoradiography, but use tissue homogenates instead of sections. This does not permit high resolution analysis as e.g. the laminar organization of receptors, but allows more reliable quantification of total receptor density, because the radioligand can reach targets in solution easily. Another advantage is that the determination of dissociation constants (K_D) can be performed with less effort and more reliably than in sections due to the fact that different concentrations of tracer can be applied simultaneously in test tubes to membrane suspensions from the same subject.

Study	n	Age (y)	Ligand	Conc. (K_D)	Non-specific Binding	Conc. (K_D)	Section Thickness (µm)
Cortes et al (1988)	16	67.9	[³H]Imipramine	7.14	Desmethylimipramine	56 818.18	10
Cortes et al (1988)	16	67.9	[³H]Paroxetine	3 846.15	Fluoxetine	12 345.68	10
Gross-Isseroff and Biegon (1988)	16	50.0	[³H]Imipramine	3.57	Amitryptiline	232 558.14	40
Chinaglia et al (1993)	8	80.9	[³H]Citalopram	0.86	Imipramine	714.29	10
Joyce et al (1993)	8	68.1	[³H]Cyanoimipramine	2.27	Desmethylimipramine	56 818.18	20
Arango et al (1995)	22	41.3	[³H]Cyanoimipramine	1.82	Sertraline	3 448.28	20
Gurevich and Joyce (1996)	15	67.6	[³H]Cyanoimipramine	2.27	Citalopram	862.07	20
Gurevich and Joyce (1996)	15	67.6	[³H]Paroxetine	1.92	Citalopram	862.07	20
Stockmeier et al (1996)	7	55	[³H]Paroxetine	2.81	Fluoxetine	1 234.57	10
Little et al (1997)	8	47.6	[¹²⁵I]β-CIT	5.10	Citalopram	86.21	16
Dean et al (1999)	10	59.7	[³H]Citalopram	2.59	Paroxetine	7 692.31	20
Bligh-Glover et al (2000)	10	53.2	[³H]Paroxetine	2.81	Fluoxetine	1 234.57	20
Mann et al (2000)	71	42	[³H]Cyanoimipramine	1.82	Sertraline	3 448.28	20
Mantere et al (2002)	10	53.5	[³H]Citalopram	1.03	Fluoxetine	1 2345.68	100
Klimek et al (2003)	11	56.5	[³H]Paroxetine	2.31	Citalopram	862.07	20
Varnas et al (2004)	5	58.0	[³H]Citalopram	1.72	Fluoxetine	12 345.68	100
Underwood et al (2012)	15	46.4	[³H]Cyanoimipramine	2.50	Sertraline	3 448.28	20

Table 1:
This list summarizes the key methodical aspects of autoradiography studies on SERT which investigate a neurologically and psychiatrically healthy adult group of subjects. The concentration of substances used is given as a multiple of the dissociation constant (K_D) specified by Tatsumi et al (1997). For Cyanoimipramine, K_D was calculated as the average of values provided in published literature (Gurevich & Joyce 1996, Joyce et al 1993, Kovachich et al 1988, Way et al 2007). For β-CIT, K_D was adapted from Eshleman et al (1999). (Conc., Concentration of ligand used given as a multiple of its dissociation constant at the serotonin reuptake transporter)

4.2 Monoamine Neuromodulatory Systems

The monoamine neuromodulatory systems are comprised of groups of neurons mostly located in the brainstem influencing many other regions of the brain. Alterations of these systems were revealed in many psychiatric and neurological disorders.

In the case of serotonin (5-HT), these neurons are located in the raphe nuclei and project to most cortical areas, subcortical regions, and the spinal cord (Hornung 2003, Lundberg et al 2005, Palkovits et al 1974). Norepinephrine (NE) neurons can be found in the locus coeruleus and have similarly broad projections (Benarroch 2009).

The 5-HT system is implicated in the regulation of mood, emotion, appetite (Haleem 1993), sleep (Franco-Perez et al 2012), processing of anxiety (Akimova et al 2009, Lanzenberger et al 2007) and a permanently growing list of crucial brain functions (Saulin et al 2012). It is involved in the mediation of reward (Kranz et al 2010)and is capable of controlling cognitive performance, as indicated by reports of impaired learning and memory in humans elicited by depletion of tryptophan, an essential precursor of 5-HT (Park et al 1994).

Trials in mice revealed the role of various 5-HT receptors in the reinforcement of actions, exploration of new environments and locomotor activity, presumably via modulation of the Dopamine (DA) system (Layer et al 1992, Rocha et al 2002). Mice lacking the 5-HT$_{1B}$ receptor showed a pronounced aggressive behaviour compared to wild type mice (Saudou et al 1994).

Autoradiography studies on 5-HT transporter (SERT) assessed significant differences of regional SERT density between controls and alcoholics (Gross-Isseroff & Biegon 1988, Mantere et al 2002), antidepressant treated patients (Cortes et al 1988), patients with Morbus Parkinson or progressive supranuclear palsy (Chinaglia et al 1993) and schizophrenics (Joyce et al 1993).

Studies on the polymorphisms in the SERT gene found among others associations of certain genotypes with major depressive disorder (MDD) (Ho et al 2012), attention deficit and hyperactivity disorder (ADHD) (Kent et al 2002), hyperkinetic disorders (Seeger et al 2001), Tourette's disorder (Moya et al 2013), schizophrenia (Li et al 2013), and irritable bowel syndrome (Kumar et al 2012). Drugs targeting SERT are used on a daily basis e.g. in the treatment of MDD (Lanzenberger et al 2012), bipolar disorder, general anxiety disorder (White et al 2005), ADHD (Popper 1997), eating disorders (McElroy et al 2012), and post-traumatic stress disorder (Abrams et al 2013).

The NE system seems to be involved in arousal, attention (Berridge & Waterhouse 2003, Devauges & Sara 1990), exploration of and coping with new environments (Aston-Jones & Cohen 2005, Yu & Dayan 2005) and therefore is hypothesized to be involved among other things in the pathogenesis of ADHD (Biederman & Spencer 1999). Human *post mortem* studies on the NE transporter (NET) found significant alterations in Morbus Alzheimer (Gulyas et al 2010, Tejani-Butt et al 1993), and a decrease of NET-binding in the LC in MDD (Klimek et al 1997) and with age (Tejani-Butt & Ordway 1992).

Dopamine (DA) projections to the striatum originate in the substantia nigra of the midbrain, whereas DA terminals in the frontal cortex and nucleus accumbens stem from the ventral tegmental area (Bjorklund & Dunnett 2007). The DA system is associated with reward processing (Schultz 1998) and drive (Flaherty 2005). Disruption of striatal DA transporter (DAT) distribution was reported ex-vivo in Morbus Parkinson, progressive supranuclear palsy, Morbus Huntington and schizophrenia (Chinaglia et al 1992, Gonzalez et al 2000). Further changes were found in cocaine addicts (Little et al 1993, Little et al 1998, Staley et al 1994) and alcoholics (Tupala et al 2001).

4.2.1 MONOAMINE REUPTAKE TRANSPORTERS

Monoamine transporters (MATs) are responsible for the uptake of their respective monoamine neurotransmitters from the extracellular fluid (Amara & Kuhar 1993) and therefore for the termination of neurotransmission mediated by these molecules. Given that MATs are mainly located perisynaptically on the presynaptic nerve terminal (Huang & Pickel 2002, Miner et al 2003, Nirenberg et al 1997, Nirenberg et al 1996), their activity contributes to the recycling of neurotransmitters, while allowing monoamine transmitters to spread beyond the synaptic cleft (Bunin & Wightman 1998, Bunin & Wightman 1999, Garris et al 1994) and presumably exert so-called
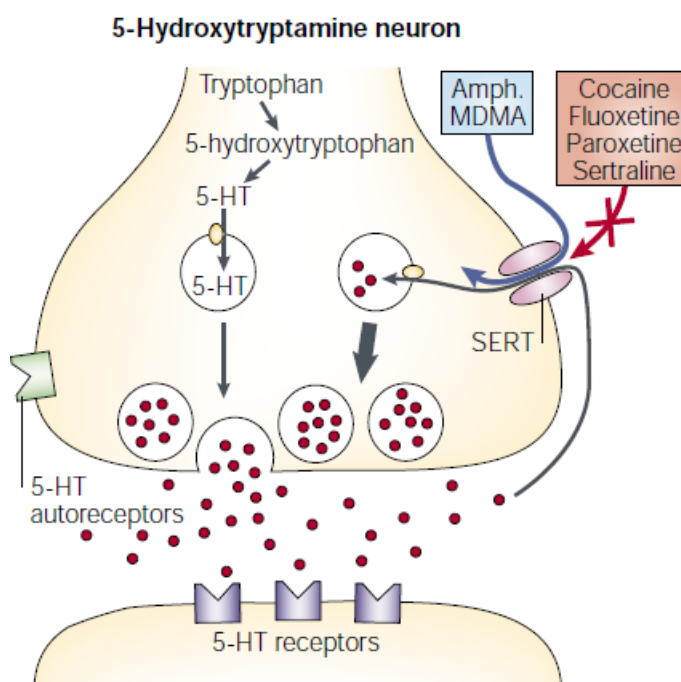
Figure 4:
Monoamine reuptake transporters are mainly located perisynaptically on the presynaptic nerve terminal. A 5-HT synapse is depicted. Common illicit and therapeutic drugs inhibiting or being a substrate of SERT are named. Tryptophan, an amino acid, is a precursor of 5-HT. Reproduced from Torres et al (2003).

volume-transmission (Agnati et al 1995). This reuptake and reuse mechanism was first described for NE in 1961 (Hertting & Axelrod 1961, Iversen 1971).

The isolation of complementary DNA launching detailed molecular characterization of the human NE transporter (NET) (Pacholczyk et al 1991) was rapidly followed by similar progress on the DA- (Giros et al 1992) and 5-HT- (Ramamoorthy et al 1993) transporters, DAT and SERT. Together with other transporter proteins, they were grouped into the solute carrier 6 gene family (SLC6). Members of this family are neurotransmitter-sodium-symporter molecules, meaning that transport of their substrates across the cell membrane is coupled to sodium and chloride ions (Borowsky & Hoffman 1995, Gu et al 1994, Gu et al 1996). Quite independently of their discovery and exploration, MATs have been the target of a vast amount of psychiatric and illicit drugs (Bonisch & Bruss 2006, Jayanthi & Ramamoorthy 2005, White et al 2005).

Although MATs display higher affinity for their eponymous substrate over other monoamines (Tatsumi et al 1997), evidence has amassed suggesting that monoamine transport is far from exclusive:

Giros et al. (1994) have shown uptake of DA by cells expressing NET only and vice versa for NE and DAT. Studies in mice either lacking SERT (Mossner et al 2006, Zhou et al 2002) or treated with selective serotonin reuptake inhibitors (SSRIs) (Zhou et al 2005) reported accumulation of 5-HT in terminals of dopaminergic neurons, which did not occur in mice also lacking DAT or treated with a DAT-selective antagonist. Furthermore, (Zhou et al 2005) and (Vizi et al 2004) demonstrated that monoamines taken up by non-corresponding transporters could be released again into the extracellular fluid. In fact, drugs selective for one of the MATs may affect extracellular concentrations of all monoamines (Reith et al 1997).

These effects are region specific and largely dependent on the proportions of available transporters, as shown in rodents for selective norepinephrine reuptake inhibitors (NRIs) which raise extracellular DA concentrations in the frontal cortex and hippocampus, areas with high NET- and low DAT- density, while having little effect on DA in the striatum, where the DAT is abundant and NET sparse (Borgkvist et al 2012, Bymaster et al 2002, Carboni et al 2006, Carboni et al 1990).

Further support for monoamine cross-uptake and differential drug effects can be derived from MAT knock-out studies (Carboni et al 2001, Moron et al 2002, Shen et al 2004, Vizi et al 2004, Xu et al 2000, Zhou et al 2002). For excellent reviews see Carboni and Silvagni (2004) or Daws (2009).

Another intersection of monoamine systems is indicated by the presumable interdependence of MAT expression: For example, Solich et al. (2011) demonstrated that SERT and DAT binding are higher in NET knockout mice. Also, Chen and Lawrence (2003) observed higher DAT binding after treatment of rats with desmethylimipramine, a NET-selective antidepressant.

Until recently, *in vivo* quantification of MATs was hindered by the slow development of specific and affine tracers that could be used in humans (Emond et al 1997, Schou et al 2004, Wilson et al 2000). Among the MATs, PET imaging of SERT is currently most advanced. A comprehensive *in vivo* databank of SERT and 5-HT receptor binding potentials was elaborated by Savli et al. (2012). Ito et al. (2008) provided a similar databank for the dopaminergic system. Imaging of NET was launched recently (Arakawa et al 2008, Logan et al 2007, Takano et al 2008) and to my knowledge, up until today only few brain regions were analysed.

In light of this evidence, there is much reason for a synoptic investigation of the monoamine neuromodulatory systems in neuroimaging.

Comprehensive binding databanks are the first step towards this goal.

4.2.2 EFFECTS OF SEX ON SERT

Five *post mortem* studies investigated the effect of sex on SERT density. Of these, two studies published by the same group reported approximately 25% higher binding in male cortices (Arango et al 1995, Mann et al 2000), while Gross-Isseroff and Biegon (1988) and Cortes et al (1988) found no difference in binding density between sexes in a large number of regions. Out of 15 *in vivo* studies, PET and SPECT, testing the influence of sex on SERT, only 4 investigated cortical regions: Jovanovic et al (2008) reported barely significant reduced SERT [^{11}C]MADAM binding in the inferior frontal gyrus and striatal ROIs and of women, and Erritzoe et al (2010) found sex to be a useful factor in a multiple regression model to predict SERT binding potential for the midbrain, but not for the cortex. Meyer et al (2004) and Praschak-Rieder et al (2008) found no significant influence on the cortex.

In summary, it can be stated that effects of sex on subcortical SERT densities are negligible, while they remain largely uninvestigated for cortical regions.

4.2.3 EFFECT OF AGE ON SERT

17 *post mortem* studies tested the effect of age on SERT density. Severson et al (1985) found an increase of [^{3}H]imipramine binding with age to membranes prepared from frontal and parietal cortices and the hypothalamus. Cortes et al (1988) reported an increase with age of [^{3}H]imipramine binding to the occipital and frontal cortex, amygdala, globus pallidus, and the central gray. However, only two young subjects were enrolled in the study and no correction for multiple comparisons was performed. Similarly, Gross-Isseroff and Biegon (1988) noted an increase of [^{3}H]imipramine binding in the amygdala, several cortical regions and the head of the caudate nucleus. Again, no correction for multiple comparisons was applied.

The remaining *post mortem* studies reported no significant influence of age on SERT density (Andersson et al 1992, Arango et al 1995, Arranz et al 1993, Dean et al 1999, Mann et al 2000, Mantere et al 2002, Rosel et al 1997). Most studies investigated cortical regions, only five studies with small sample sizes measured SERT binding in brainstem or striatal regions (Bligh-Glover et al 2000, Lawrence et al 1997, Lawrence et al 1998, Little et al 1997, Stockmeier et al 1996).

In contrast, these regions are the most appraised *in vivo*:

For the brainstem as a whole only one study investigating the influence of age on binding of a specific tracer is available and reports no significant effect (Ho et al 2012). Four authors used [^{123}I]β-CIT to determine SERT in a total of 220 subjects and found a significant decrease of tracer binding in brainstem with age (Hesse et al 2003, Jacobsen et al 2000, Pirker et al 2000, van Dyck et al 2000), while Heinz et al (1998) (13 subjects) and Staley et al (2006) (32 subjects) did not.

11 out of 13 *in vivo* studies used specific tracers to elucidate changes of midbrain SERT density with age. 5 of these studies with a total of 203 subjects reported a significant decrease of SERT with age (Erritzoe et al 2010, Ichimiya et al 2002, Newberg et al 2005, Praschak-Rieder et al 2008, Yamamoto et al 2002). The remaining studies with a total of 139 subjects reported no significant effect (Cannon et al 2006, Frankle et al 2005, Ho et al 2012, Meyer et al 2004, Oquendo et al 2007, Reimold et al 2008).

16 PET and SPECT studies investigated the effect of age on the binding of various SERT tracers in the thalamus or diencephalon. 11 found a significant decrease of SERT with age (Cannon et al 2006, Erritzoe et al 2010, Hesse et al 2003, Ichimiya et al 2002, Kalbitzer et al 2009, Pirker et al 2000, Praschak-Rieder et al 2008, Reimold et al 2008, Staley et al 2006, van Dyck et al 2000, Yamamoto et al 2002), the remaining studies reported only tendencies (Frankle et al 2005, Jacobsen et al 2000, Meyer et al 2004, Oquendo et al 2007).

9 *in vivo* studies investigated the effect of age on SERT binding in striatal regions. Two of these studies used [^{123}I]β-CIT which has a considerable affinity for DAT and reported a significant decline of binding with age (Jacobsen et al 2000, Pirker et al 2000). Out of the remaining studies, using the SERT specific tracers [^{11}C]DASB and [^{123}I]ADAM, four with a total subject number of 79 reported no significant change in tracer binding in striatal regions with age (Cannon et al 2006, Frankle et al 2005, Ho et al 2012, Meyer et al 2004), while three studies with a total of 165 subjects did (Erritzoe et al 2010, Meyer et al 2001, Praschak-Rieder et al 2008).

For cortical regions evidence is sparse. If the influence of age is tested for at all, only few small parts, such as the anterior cingulate cortex (Cannon et al 2006, Frankle et al 2005, Meyer et al 2004, Oquendo et al 2007) or anteromedial prefrontal cortex (Praschak-Rieder et al 2008), or gross structures, such as the neocortex (Erritzoe et al 2010) are analysed.

Taken together, there is good reason to believe in a steady decline of striatal, thalamic, midbrain and brainstem SERT density with age.

At the same time, the effects of age on SERT in cortical regions need to be explored. Moreover, it is worthwhile to find out which parts of the brainstem account for most of the decline of SERT with age. Especially the raphe nuclei should be appraised in this context.

4.3 Study Aims & Relevance

4.3.1 SEROTONIN TRANSPORTER BINDING POTENTIAL DATABASE

To my knowledge there is only one comprehensive databank of human *in vivo* PET data on SERT available, published recently by our group (Savli et al 2012), including a subgroup (18 subjects) of the current study. Therefore, the main objective of this project was to provide binding potential (BP) values for brain regions delineated according to the classical Brodmann (1909) parcellation scheme and Automated Anatomical Labelling (AAL) regions (Tzourio-Mazoyer et al 2002) as well as voxel-wise parametric maps. Despite the opportunity to see the topology and study the function of this transporter, such a databank could serve as a reference for future PET-studies e.g. studies with a small sample size. Moreover, studies applying other neuroimaging techniques could use this databank for multimodal interpretation of their own results (Savli et al 2012). Especially pharmacological functional MRI (fMRI) imaging studies can profit from this data using it for prediction and interpretation of drug effects on regional brain activation.

4.3.2 SEX AND AGE EFFECTS

The effects of sex and age on total and ROI-specific SERT binding are crucial for correction if other factors are under investigation. Still, data is inconsistent between studies. Especially, *post mortem* and *in vivo* binding values diverge: the former tend to report a SERT increase with age, while the latter show the opposite. Therefore, testing for these demographic variables in our large sample was expected to further clarify this matter and yield correction-values for the comparison of *in vivo* and *post mortem* data.

4.3.3 COMPARISON WITH ABSOLUTE TRANSPORTER DENSITY

I hypothesized that PET BPs for SERT correlate with corresponding transporter densities given in pmol/g tissue derived from *post mortem* autoradiography data. Regression models between PET-binding potentials and *post mortem* autoradiography data allow inferences on absolute receptor densities from *in vivo* data. Such regression models if available for different tracers would make the direct comparison of the absolute *in vivo* abundance of their respective target molecules possible.

Applying this method to SERT, the chief target of a vast amount of psychotropic drugs, may facilitate understanding and future investigation of the action of psychiatric medication.

4.4 Hypotheses

1. Significant and valid regression models can be obtained using i*n vivo* SERT binding potentials and *post mortem* absolute binding values (pmol/g) adapted from published data allowing the calculation of regional binding densities, B_{max}, from BP.

2. There is a ROI-specific influence of age on SERT binding potentials.

3. Binding potentials for SERT differ between sexes in certain ROIs.

5 METHODS & MATERIALS

5.1 Study Funding

Data for the current investigation was obtained from healthy control groups enrolled in the following projects of our group:

4. The influence of sex steroid hormones on serotonin transporter binding in the human brain investigated by PET. Funding: Austrian National Bank, Jubiläumsfonds Project # 13214, 2009 – 2012, EK: 620/2008

   Principal Investigator: Assoc. Prof. PD Dr. Rupert Lanzenberger

5. The Serotonin Transporter in Attention Deficit Hyperactivity Disorder Investigated with Positron Emission Tomography. Funding: Austrian National Bank, Jubiläumsfonds Project# 13675, 2010 – 2012, EK: 784/2009

   Principal Investigator: PD Mag. Dr. Markus Mitterhauser, Department of Nuclear Medicine, Co-Investigator: Assoc. Prof. PD Dr. Rupert Lanzenberger

These studies were conducted in cooperation of the Department of Nuclear Medicine (PET measurements and radioligand synthesis) and the Department of Psychiatry and Psychotherapy at the Medical University of Vienna, Austria.

5.2 Subjects

Healthy control subjects were recruited via advertisements for the above mentioned projects of our group.

5.2.1 INCLUSION CRITERIA

- Age 18 to 55 years when giving informed consent.
- Physical health.
- Understand and willingness to sign the written informed consent form.

5.2.2 EXCLUSION CRITERIA

- Severe somatic diseases.
- History of or current treatment with psychiatric medication e.g. stimulants, selective norepinephrine or serotonin reuptake inhibitors.
- Use of alcohol, drugs of abuse, or medication in a manner indicative of chronic abuse or satisfying DSM-IV-TR criteria for alcohol or other substance dependence.
- Current psychiatric disorder (Axis I or Axis II diagnosis according to DSM-IV-TR).
- Pregnancy (Positive urine pregnancy test), breast feeding.
- Participation in studies with PET or SPECT within the last 10 years.

The exclusion criteria were selected to assure safety for participants and eliminate the confounding effect of medical conditions, medication and drugs presumably altering the monoaminergic systems on results of PET measurements.

5.2.3 STANDARD EXAMINATIONS

The screening visit consisted of a somatic and psychiatric examination including blood sampling for routine parameters, an electrocardiogram, a urine pregnancy test (HCG), a drug screening and the Structured Clinical Interview for DSM-IV Diagnosis (SCID). The drug screening (urine analysis and anamnesis) covered the following substances: barbiturates, benzodiazepines, buprenorphine, amphetamine, ketamine, cocaine, THC, methadone, methamphetamine, methyl-enedioxy-methylamphetamine (ecstasy), morphine, phencyclidine, kotinine (DIPRO DRUGLAB, Dipromed Handels GmbH. / A, Multi-drug screen test panel 10/2: AMP-BAR-BZO-COC-mAMP-MOP/OPI-MTD-MDMA-THC-TCA). Another urine pregnancy test was applied before the PET measurement. Within 14 days after the PET scan a final medical examination was conducted.

5.3 Positron Emission Tomography Imaging Procedures

Each subject underwent one PET scan using a GE Advance PET tomograph (GE Medical Systems, Wukesha, WI) at the Medical University of Vienna as in previous studies from our group.

Tracers were provided, synthesized and controlled by the Department of Nuclear Medicine, PET Centre, Medical University of Vienna. [^{11}C]DASB ([^{11}C]-N,N-dimethyl-2-(2-amino-4-cyanophenylthio)-benzylamine) was synthesized complying with procedures developed by Solbach et al (2004) as published by Häusler et al. (2009). The whole preparation ran automatically in a lead shielded hot cell. Quality control was assessed obeying standard procedures routinely performed at the PET Centre.

Emission scans started concurrently with intravenous bolus injection of [^{11}C]DASB following a standard protocol realized at the PET Centre. The [^{11}C]DASB target dose was set at 4.7 MBq/kg body weight. Dynamic PET scans were acquired in 3D mode during a total scan time of 90 minutes as customized to modelling considerations (Ginovart et al 2001, Ogden et al 2007).

The emission data was scatter corrected using 35 contiguous slices (matrix 128*128), reconstructed with a slice thickness of 4.25mm and a spatial resolution at the center of the field of view of 4.36mm full-width at half-maximum (FWHM).

5.4 Data Processing & Statistics

SPSS 19.0 (for ROI-based data, descriptive statistics, diagrams, correlations and regressions; SPSS Inc., Chicago, IL, USA, www.spss.com), Microsoft Excel 2013 (for simple calculations and polar charts) and SPM8 (for parametric voxel-wise analysis, http://www.fil.ion.ucl.ac.uk/spm/software/spm8/) were used for statistical analyses. BP calculation was carried out in PMOD 3.0 (PMOD Technologies Ltd, Zürich, Switzerland).

All processing steps from raw data to ROI- and voxel-BP were carried out as seen in Savli (2012). PET scans were visually inspected and motion corrected using SPM8, and then normalized to a tracer-specific template to enable automated ROI analysis, as described previously by our group (Stein et al 2008). Smoothing was carried out with an isotropic 8 mm Gaussian kernel. Eventually, normalization of each dynamic scan was evaluated visually and corrected if deemed necessary.

Time activity curves were obtained by applying a ROI-template to each scan via an in-house MATLAB program. The kinetic modeling tool PKIN implemented in PMOD and the "multilinear reference tissue model" (MRTM/MRTM2) were used to calculate binding potentials (BP_{ND}) (Ichise et al 2003). The cerebellar grey matter except for the vermis was used as the reference region (Parsey et al 2006), since it has been reported to be virtually free from SERT (Kish et al 2005). Thalamus, a SERT rich region, was used to estimate clearance rate, k_2', with MRTM.

5.4.1 BINDING POTENTIAL DATA

In the current investigation a standardized ROI-template comprising the classical cytoarchitectonic Brodmann (1909) parcellation scheme (41 regions) and the Automated Anatomical Labeling (AAL) atlas (Tzourio-Mazoyer et al 2002) complemented by subcortical ROIs (52 regions) were used as described by (Savli et al 2012). Brainstem ROIs were drawn on axial planes as shown in Figure 5. This approach sacrifices power in favour of expeditious data processing, avoiding bias due to manual ROI delineation.

Additionally, parametric voxel-wise maps were calculated by determining the BP for each voxel and brain and then averaging brain maps. All ROIs are listed in Table 10 in the appendix. Results were presented by means of descriptive statistics: arithmetic mean, standard deviation (SD), range and polar diagrams, one for each of the two parcellation schemes. Total *in vivo* binding was calculated by adding the BPs of all non-overlapping ROIs listed in Table 10 (AAL and subcortical) multiplied by their respective volume, then dividing the result by the sum of these ROIs' volumes.

Figure 5:
The positioning of brainstem ROIs on top of a BP mean image obtained from 30 healthy subjects is depicted in axial, coronal and sagittal planes. Crossbars meet in the center of the dorsal raphe ROI (black). Note the overlap of the 2 voxels marked by the crossbar between the midbrain and dorsal raphe ROIs. The median raphe nucleus is marked in dark red. The midbrain ROI is pink
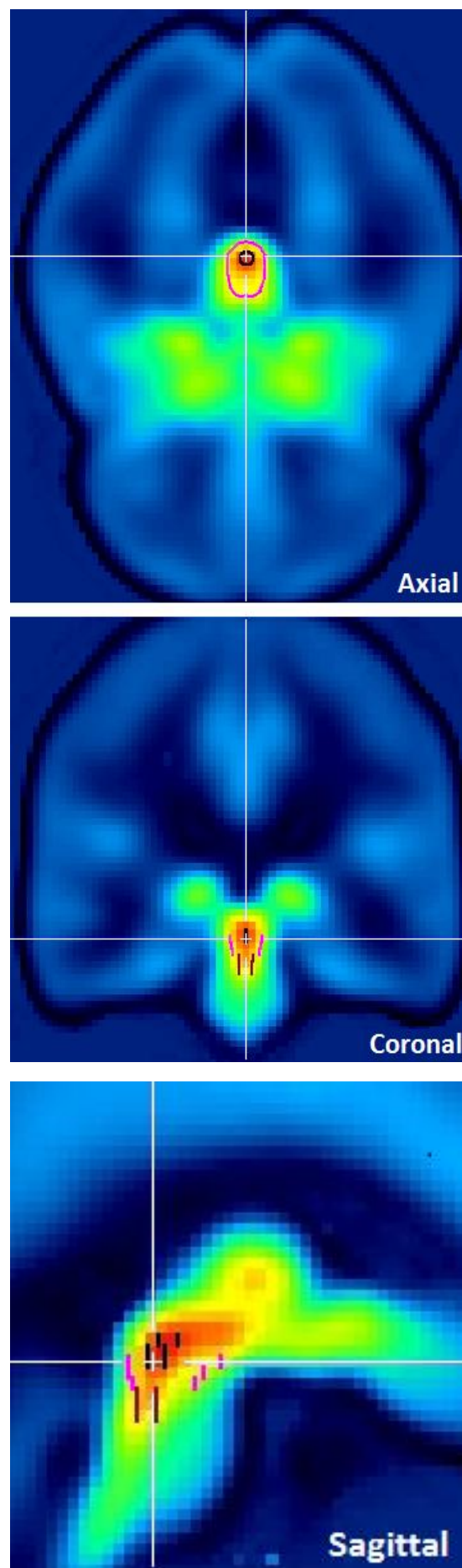
5.4.2 EFFECTS OF SEX AND AGE

To investigate the effect of sex on SERT binding simple t-tests were calculated for total and 52 ROI (AAL and subcortical) BPs. Normal distribution of values was assessed visually in histograms and using Kolmogorov Smirnov tests. To visualize the differences, box-plots for ROIs with the most pronounced influence of sex were generated. Pearson and Spearman correlation coefficients were calculated between total- and ROI BPs and age. The level of significance was set at $\alpha \leq 0.05$. Correction for multiple comparisons was carried out by multiplying p-values with the number of ROIs tested (52), i.e. with Bonferroni correction.

5.4.3 COMPARISON WITH ABSOLUTE TRANSPORTER DENSITY

To compare *in vivo* BPs with absolute SERT density, *post mortem* B_{max} data from published human autoradiography studies was collected via PubMed.

Since these studies seldom used standardized parcellation schemes, in most cases several ROIs had to be adjusted in order to become amenable to direct comparison with PET data. The most common transformation consisted in averaging ROI BPs, considering the ROI-volume to match a larger region characterized *post mortem* (e.g. frontal cortex). On the other hand, wherever necessary, small regions evaluated *post mortem* were pooled, considering their respective volume to estimate SERT binding density of the superordinate structure that they are part of, e.g. midbrain or striatum. Detailed information on how ROIs were matched are included in the appendix (page 59).

If more than 3 ROIs from a published autoradiography study could be matched with PET data in this manner, the study was included in analysis. Pearson product moment and Spearman rank correlation coefficients were calculated between mean ROI SERT BP values and topologically corresponding *post mortem* transporter densities given in pmol/g tissue for each subset of published data. Level of significance was set at $\alpha \leq 0.05$. Scatter plots were drawn. Regression models were generated if correlation was significant. Residuals were checked for normal distribution in histograms. Additionally, residual plots were drawn to control for heteroscedasticity and possible linear or non-linear factors. Extreme outliers were excluded in final regression models if partial volume effects or poor agreement between *post mortem* and *in vivo* regions seemed probable.

As a last step, B_{max} values were corrected to account for the different age of subjects in the *post mortem* study populations. This was accomplished by applying correction factors calculated from published studies as explained in Table 2 and the following equation to B_{max} values from each autoradiography study:

$$B_{max\prime} = \frac{B_{max}}{(1-a)^{\frac{\Delta age}{10}}} \qquad (8)$$

$B_{max\prime}$ denotes the age corrected binding value, a is the relative decrease of binding per decade (Table 2), Δage is the difference between mean age of the *post mortem* and the PET study population.

The linear equations obtained with age corrected values were used to estimate absolute SERT binding density for all ROIs measured *in vivo*. These results were visualized as polar coordinate systems.

Study	n	Tracer	Decrease per decade (%)
Thalamus			5.1[a]
Cannon et al (2006)	37	[11C]DASB	4.5
Erritzoe et al (2010)	60	[11C]DASB	1.4[b]
Reimold et al (2008)	19	[11C]DASB	6.4[b]
Yamamoto et al (2002)	28	[11C]McN5652	9.6
Midbrain			4.7[a]
Erritzoe et al (2010)	37	[11C]DASB	4.5
Newberg et al (2005)	6	[123I]ADAM	3
Yamamoto et al (2002)	28	[11C]McN5652	10.5
Striatum			3.6[a]
Erritzoe et al (2010)	60	[11C]DASB	1.9[c]
Pirker et al (2000)	35	[123I]β-CIT	6.6[d]

Table 2:
Age correction factors (decrease per decade) were calculated using published decrease values from *in vivo* SERT imaging studies.
[a] ROI age correction factors were calculated by multiplying the relative decrease values given for each study by the number of subjects included, adding results, then dividing by the number of all subjects. Correction factors for the putamen and caudate nucleus are not shown.
[b] Relative decrease values were obtained by dividing absolute decrease by mean ROI BP published in the respective study.
[c] Relative decrease value was obtained by dividing absolute decrease by mean ROI BP of striatal ROIs published in the respective study, then averaging taking into account the respective ROI volumes.
[d] Due to limited data on striatal SERT binding and age, a study using [123I]β-CIT, a ligand not selective for SERT was included.

5.5 Ethics

The study protocols were approved by the ethics committee of the Medical University of Vienna, Austria (www.meduniwien.ac.at/ethik) (EK: 620/2008; 784/2009). The studies were completed in accordance with the Declaration of Helsinki (1964), the Austrian Arzneimittelgesetz and the EC-GCP guidelines. All subjects gave written informed consent prior to inclusion in the studies and were insured by the Department of Psychiatry and Psychotherapy, Division for Biological Psychiatry, obeying §32 of the Austrian Medicines Act.

6 RESULTS

6.1 Demography

30 Subjects (11 women), aged 18-54 years (mean 31.1 ± 10.0) were included in the current investigation. Kolmogorov Smirnov tests for age did not indicate significant deviation from normal distribution in the whole group, as well as in the male and female subgroups. A t-test for age comparing sex groups was not significant (p = 0.56). Details can be found in Table 3 and Figure 6.

Group	n	Mean age (y) ± SD	Range (y)
All subjects	30	31.13 ± 9.96	19 - 54
Women	11	31.09 ± 10.72	19 - 49
Men	19	31.16 ± 9.79	19 - 54

Table 3:
Demography of subjects.
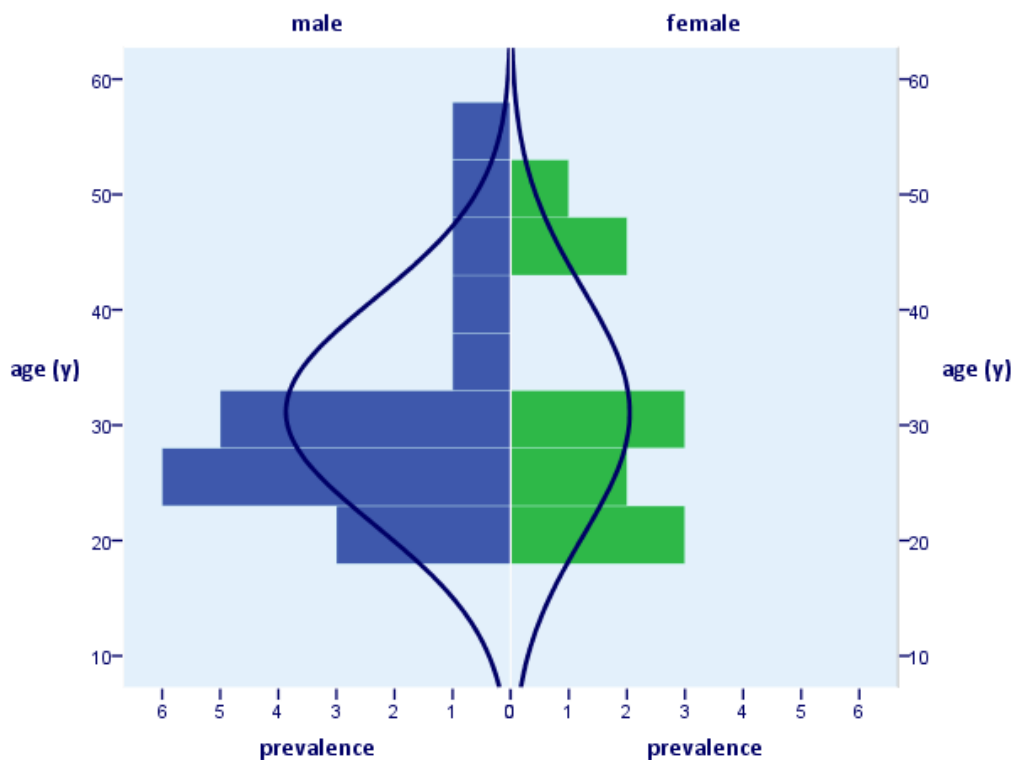
Figure 6:
Distribution of age in the study population approximated normal distribution.
(Prevalence, number of subjects)

6.2 Serotonin Transporter Binding Potential

SERT Binding potentials for ROIs defined by AAL (52 ROIs) and Brodmann (41 ROIs) parcellation schemes are given in Table 10 (page 59) and visualized in Figure 8 and Figure 9, respectively. Kolmogorov Smirnov tests did not indicate significant deviation of BP measures from normal distribution in any ROI investigated, neither in the whole sample, nor in male or female subsamples. Highest binding values were seen in subcortical regions, notably in the raphe nuclei, followed by midbrain, nucleus accumbens, and thalamus. Among cortical regions, the entorhinal area (Brodmann areas 28 and 34), olfactory cortex, subgenual cingulate cortex (corresponding to Brodmann area 25) and Insula show the most pronounced binding potentials. The very same ROIs show the greatest variance in BP values.
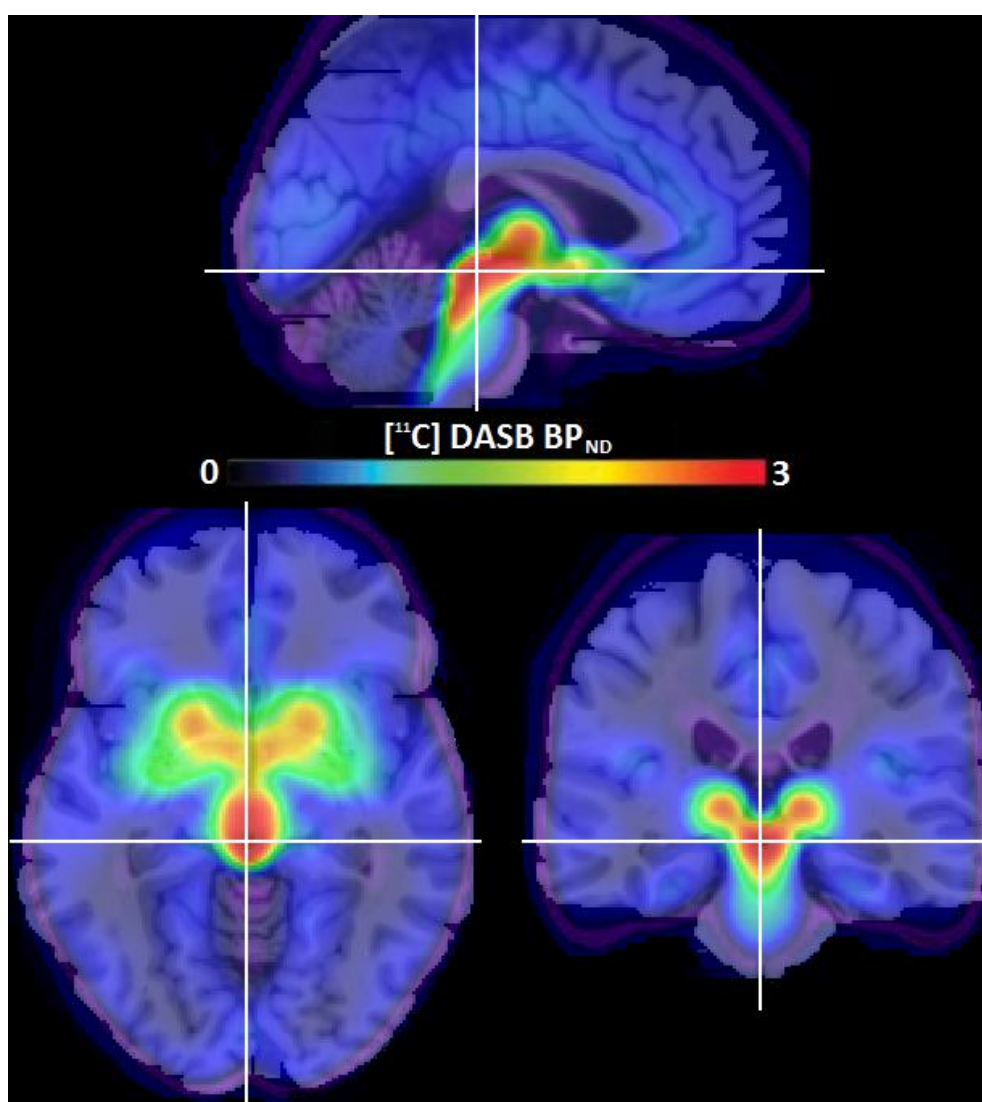
Figure 7:
Mean images of SERT BP in sagittal, axial and coronal planes obtained as described in the methods section for 30 healthy subjects. Crossbars intersect in the dorsal raphe nucleus. For orientation, binding images were overlaid onto a single subject T1 weighted MRI of a standard brain in MNI space. Corresponding ROI BP_{ND} values can be found in Table 10.
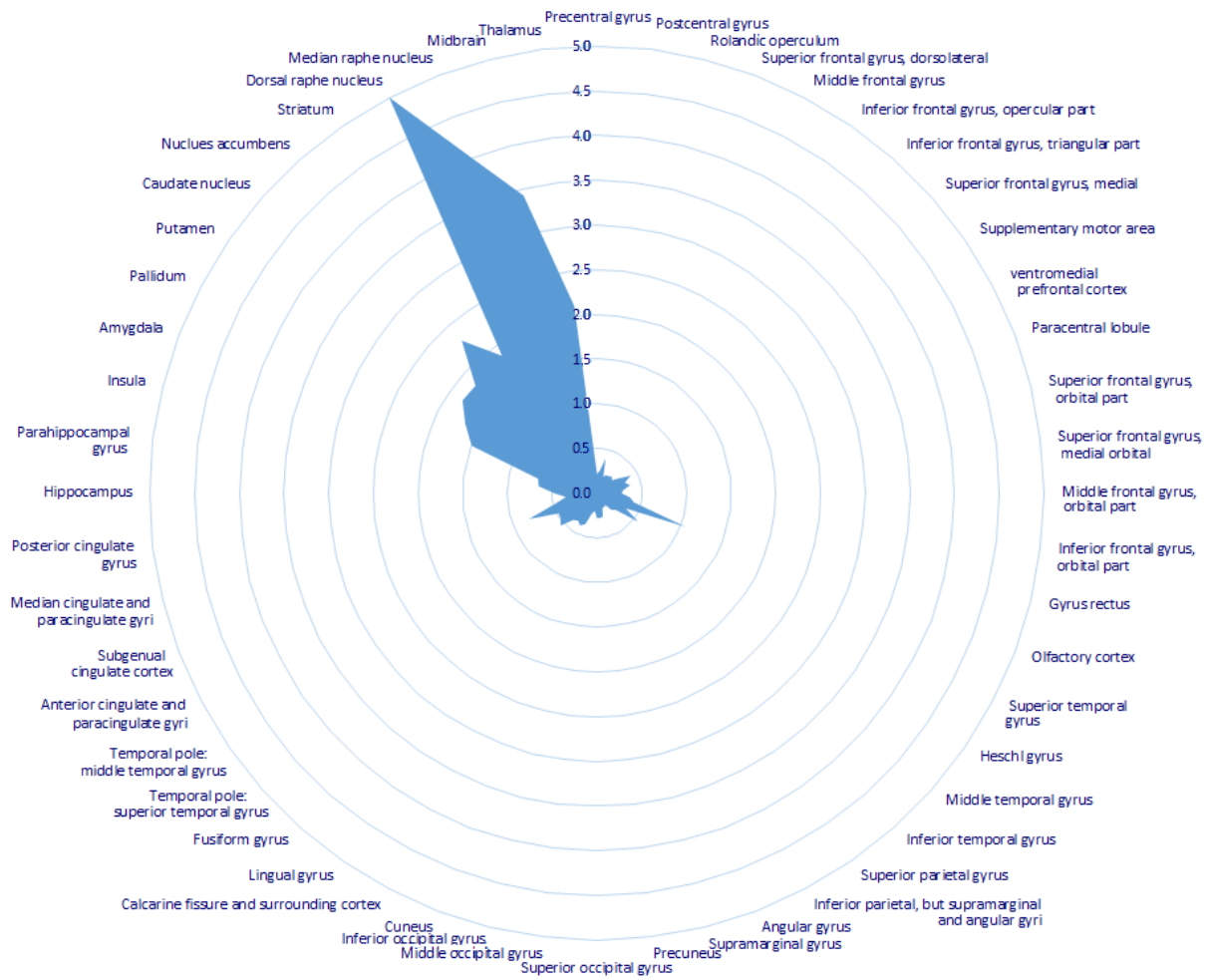
Figure 8:
SERT BP for AAL and subcortical ROIs (see Table 10 for numeric values) are plotted in this polar chart. Highest values can be seen in subcortical regions. Among cortical ROIs, the olfactory cortex and the subgenual cingulate cortex lead.
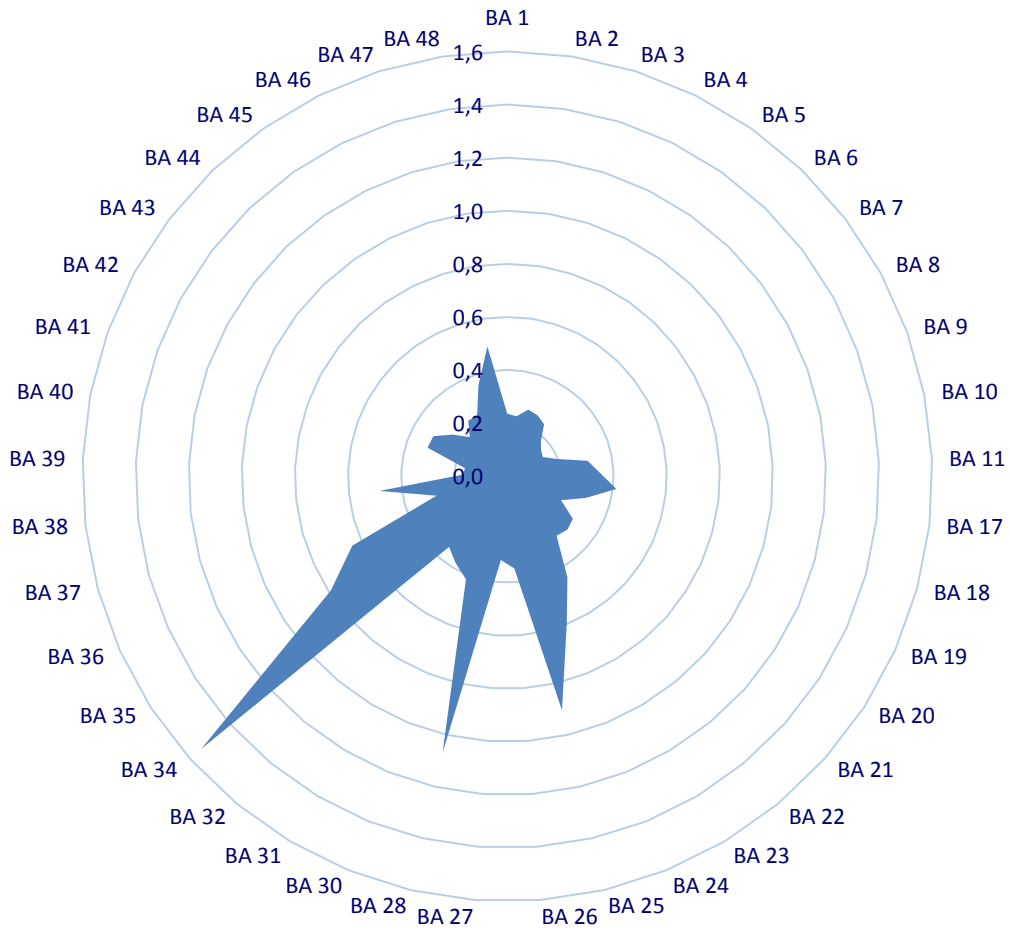
Figure 9 :
SERT BP for Brodmann areas (see Table 10 for numeric values) are plotted in this polar chart. Highest values can be seen in BA 34, 28 (entorhinal area) and 25 (subgenual area).

6.3 Sex and Age Effects

The effects of sex on age on SERT BP in AAL and subcortical ROIs, as well as on whole brain binding were investigated using t-tests, and Pearson and Spearman correlation analyses. After Bonferroni correction none of the results remained significant. Therefore, as an additional exploratory point, effects of age on BPs were assessed in males and females separately. Again, Bonferroni correction rendered most effects insignificant. Nevertheless, the following tendencies were observed: Slightly higher BP in the subgenual cingulate cortex and gyrus rectus in men (ANOVA uncorrected $p = 0.05$ and $p = 0.10$, respectively; Figure 10 and Figure 11).

In the whole sample, the strongest association of a decrease in SERT BP with age was noted in the Heschl gyrus (Pearson and Spearman correlation coefficients −0.47 and −0.40, uncorrected $p = 0.01$ and $p = 0.03$, respectively; Figure 12). All regions in which SERT binding might be influenced by subjects' age, as indicated by uncorrected p-values ≤ 0.05 for Pearson product moment or Spearman rank correlation, were summarized in Table 4.

In the male subgroup ($n = 19$), as in the whole group, the same tendency of decreasing binding in the Heschl gyrus with age was observed (uncorrected $p = 0.03$). In females, despite the small sample size ($n = 11$), correlation analysis yielded uncorrected p-values ≤ 0.05 in a broader range of regions (Table 5). Note that significance of nonparametric correlation of age and binding in the paracentral lobule of women remains significant after Bonferroni correction (corrected $p = 0.03$; Figure 13).
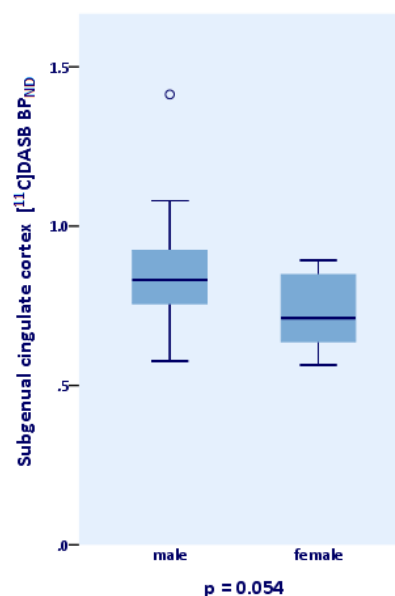
Figure 10:
Higher BP in subgenual cingulate cortex of men (mean BP = 0.86) vs. women (mean BP = 0.73), uncorrected p = 0.05.
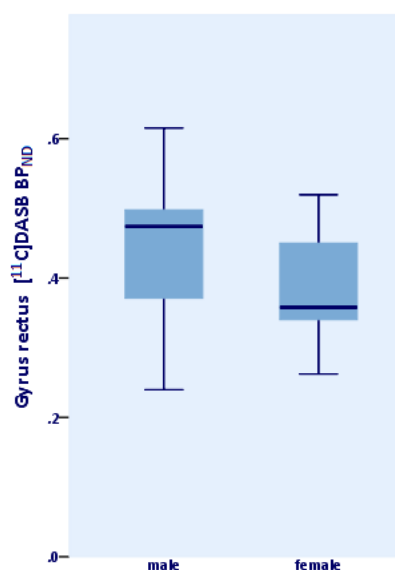
Figure 11:
Higher BP in gyrus rectus of men (mean BP = 0.45) vs. women (mean BP = 0.39), uncorrected p = 0.10.
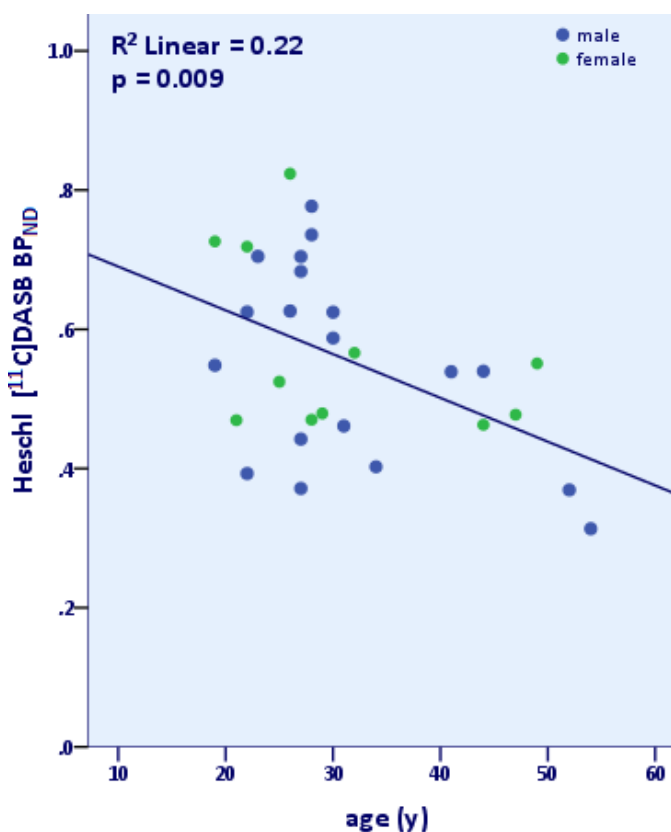
Figure 12:
A decrease in SERT BP of 0.06 per decade was noted in the Heschl gyrus (uncorrected p = 0.009; R² = 0.22).

Region of interest (AAL)	Pearson r	p	Spearman ρ	p
Heschl gyrus	−.47 **	.01	−.40 *	.03
Operculum rolandicum	−.37 *	.05	−.34	.06
Postcentral gyrus	−.33	.08	−.37 *	.04
Dorsal raphe nucleus	.39 *	.03	.26	.17
Thalamus	−.33	.07	−.36 *	.05

Table 4:
SERT BP was correlated with age using Pearson product moment and Spearman rank correlation. ROIs with a potential influence of subjects' age on binding are listed. p-Values included in this table are not corrected for multiple testing.
(*, uncorrected p < 0.05; **, uncorrected p < 0.01)
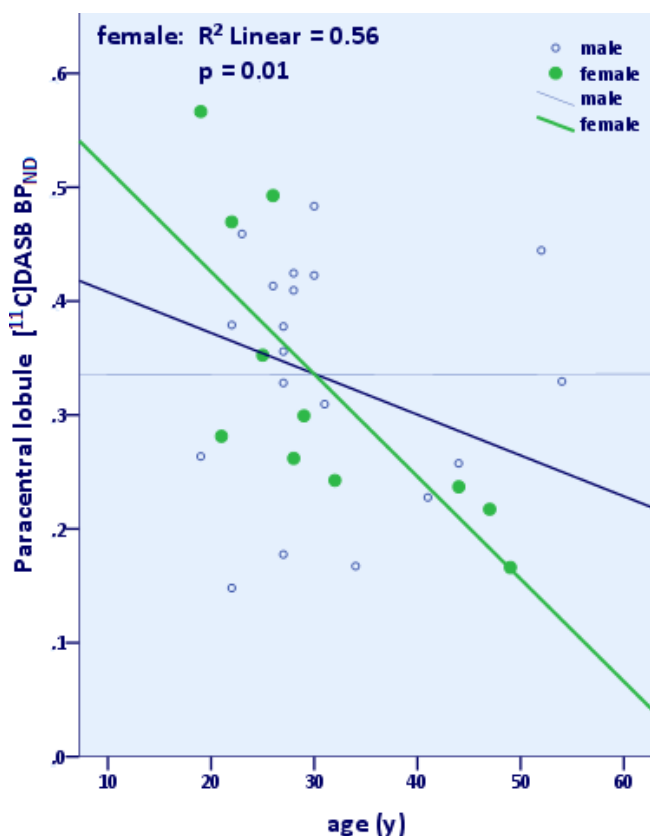
Figure 13:
SERT BP showed a decrease of 0.09 per decade in women (uncorrected p = 0.008), but not in men.
Correlation coefficients:
Pearson   −0.75   p = 0.01
Spearman   −0.86   p = 0.0006
Spearman   corrected p = 0.03
(If not specified, p-values are not corrected.)

Region of interest (AAL)	Pearson r	p	Spearman ρ	p
Men (n = 19)				
Heschl gyrus	−.49 *	.03	−.40	.09
Women (n = 11)				
Paracentral lobule	−.75 **	.01	−.86 ***	.001
Supplementary motor area	−.60	.05	−.69 *	.02
Precunes	−.68 *	.02	−.76 **	.01
Cuneus	−.61 *	.05	−.65 *	.03
Lingual gyrus	−.65 *	.03	−.61 *	.05
Median cingulate and paracingulate gyri	−.68 *	.02	−.69 *	.02
Posterior cingulate gyrus	−.60 *	.05	−.66	.03
Median raphe nucleus	.61 *	.05	.12	.71

Table 5:
SERT BP was correlated with age using Pearson product moment and Spearman rank correlation for each sex group separately. ROIs with p-values below 0.05 for correlation of binding with age are listed. p-Values included in this table are not corrected for multiple testing. Binding potentials in the paracentral lobule of women significantly decrease with age (corrected p=0.03 for Spearman rank correlation).
(*, uncorrected p < 0.05; **, uncorrected p < 0.01; ***, uncorrected p < 0.001)

6.4 Comparison with Absolute Transporter Density

Since analysis of sex and age effects on SERT BP yielded no significant results for ROIs included in the current analysis, a priori no corrections were made to account for the different demography of subjects enrolled in the *post mortem* studies.

Kolmogorov Smirnov tests and visual inspection of scatter-plots were carried out for each autoradiography study in order to find significant deviation from normal distribution of mean *post mortem* binding densities of ROIs matched with our *in vivo* PET data. Only data from Varnas et al (2004) did not fit normal distribution if midbrain and dorsal raphe nucleus, regions of high SERT density, were included in analysis.

Results of correlation of mean *post mortem* binding densities (B_{max}), assessed with radioligands highly selective for the serotonin reuptake transporter, with *in vivo* SERT binding potentials are presented in Table 6. Except for values provided by Gross-Isseroff and Biegon (1988), absolute binding densities from published studies were in excellent agreement with PET BP_{ND}. Scatter plots for mean BP_{ND} and B_{max} for each autoradiography study can be found on the following pages (Figure 14 to Figure 22).

(Model #) Post mortem study	ROIs	Radioligand	Pearson r	p	Spearman ρ	p
(1) Cortes et al (1988)	15	[³H]Imipramine	.88 ***	<10⁻⁴	.94 ***	10⁻⁷
Cortes et al (1988)	9	[³H]Paroxetine	.91 ***	<10⁻³	.97 ***	<10⁻⁴
Gross-Isseroff and Biegon (1988)	18	[³H]Imipramine	.04	.89	.02	.94
(2) Chinaglia et al (1993)	11	[³H]Citalopram	.86 ***	<10⁻³	.92 ***	<10⁻⁴
(3) Joyce et al (1993)	11	[³H]CN-IMI	.95 ***	10⁻⁵	.75 **	.01
(4) Arango et al (1995)	7	[³H]CN-IMI	.82 *	.02	.85 *	.02
(5) Gurevich and Joyce (1996)	23	[³H]CN-IMI	.91 ***	10⁻⁹	.92 ***	<10⁻⁹
(6) Gurevich and Joyce (1996)	12	[³H]Paroxetine	.89 ***	<10⁻³	.92 ***	<10⁻⁴
Mann et al (2000)	4	[³H]CN-IMI	.92	.08	1	.
(7) Varnas et al (2004)	17	[³H]Citalopram	.84 ***	<10⁻⁴	.82 ***	<10⁻⁴

Table 6:
Mean *post mortem* absolute SERT binding densities (B_{max}) were correlated with mean SERT binding potentials for each autoradiography study separately. High agreement between B_{max} and BP_{ND} was found in most cases and yielded highly significant results for studies with B_{max} values for a sufficient numbers of ROIs provided.
(Model # refers to the number of regression model given in Table 7; CN-IMI, Cyanoimipramine; *, p < 0.05; **, p < 0.01; ***, p < 0.001)

6.4.1 REGRESSION MODELS: FROM BINDING POTENTIALS TO ABSOLUTE BINDING

To make the calculation of absolute SERT density (B_{max}) values from *in vivo* binding potentials possible, linear regression models were calculated between BP_{ND} and B_{max} (pmol/g tissue), as assessed with selective radioligands in *post mortem* studies. This was performed for autoradiography data correlating significantly with mean BP_{ND} (Table 6).

For data by Cortes et al (1988), Chinaglia et al (1993), Gurevich and Joyce (1996) and Varnas et al (2004) scatter plots suggested a non-linear relationship between mean BP_{ND} and B_{max}. Also, quadratic regression models showed a better fit over linear models, implied by significant F-tests. However, after exclusion of the raphe nuclei, regions susceptible to partial volume effects, and the midbrain which was topologically poorly fit to its *in vivo* ROI (see appendix, page 64), the relationship between B_{max} and BP for the remaining ROIs was predominantly linear. This circumstance is demonstrated using scatter plots for the respective studies (e.g. Figure 14). Unfortunately, excluding these ROIs rendered regression models calculated for B_{max} values of [³H]paroxetine provided by Cortes et al (1988) insignificant. Thus, 7 linear equations to calculate *post mortem* SERT density, assessed with different radioligands, from PET BP_{ND} were obtained (Table 7).
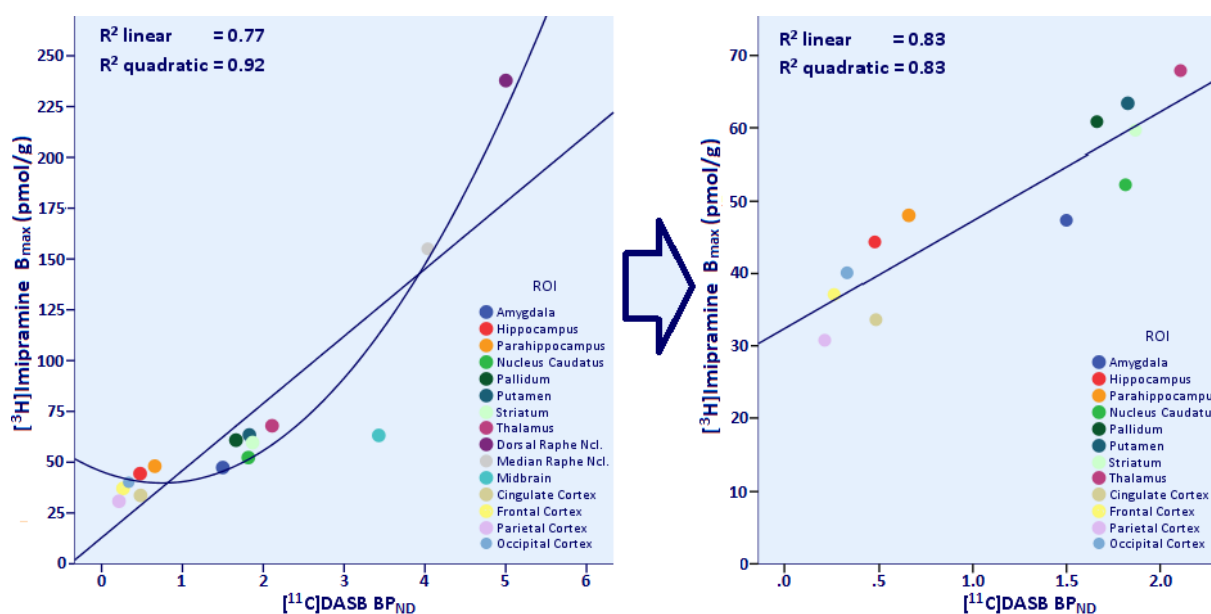
Figure 14:
Scatter plots and R² values indicated a non-linear relationship between mean SERT binding potentials and absolute [³H]imipramine binding (Cortes et al 1988), if all ROIs initially matched *post mortem − in vivo* were taken into account (left panel). This was supported by a significant F-test quadratic vs. linear regression model (ΔF = 22.6; p < 0.001). If midbrain and raphe nuclei were excluded, however, no significant advantage (ΔF = 0.09; p = 0.78) of non-linear over linear models could be seen (right panel).
(Ncl., Nucleus)

As a last step, age corrected B_{max} values were used to calculate regression models (Table 8). This improved 4 of 7 models significantly, 2 models were improved, but not significantly, and one model was left unchanged (Table 9). Age-corrected models were used to calculate B_{max} (pmol/g tissue) values using mean SERT binding potentials for all AAL, Brodmann and subcortical ROIs (Table 10). Figure 23 and Figure 24 present these results as polar charts.

The regression equation takes the form: **-binding = (slope) × [^{11}C]DASB BP$_{ND}$ + (intercept)**

Model #	R^2	p	-binding (pmol/g)	slope	intercept
1	.83	$<10^{-4}$	[^{3}H]Imipramine	14.9	32.4
2	.68	.01	[^{3}H]Citalopram	4.1	4.2
3	.89	$<10^{-4}$	[^{3}H]CN-IMI	20.9	4.0
4	.68	.02	[^{3}H]CN-IMI	20.0	4.4
5	.86	$<10^{-9}$	[^{3}H]CN-IMI	16.1	2.3
6	.77	$<10^{-3}$	[^{3}H]Paroxetine	10.8	3.0
7	.44	$<.01$	[^{3}H]Citalopram	4.1	5.4

Table 7:
Linear regression models from SERT BP$_{ND}$ to B$_{max}$ (pmol/g tissue) were calculated for each autoradiography study separately. Midbrain and raphe ROIs were excluded from regression analyses. Model # refers to the respective *post mortem* study, as specified in Table 6.

Model #	R^2	p	-binding (pmol/g)	slope	intercept
1	.86	$<10^{-4}$	[^{3}H]Imipramine	21.1	29.6
2	.77	$<.01$	[^{3}H]Citalopram	5.6	3.6
3	.90	$<10^{-5}$	[^{3}H]CN-IMI	25.1	2.3
4	.68	.02	[^{3}H]CN-IMI	20.0	4.4
5	.91	$<10^{-11}$	[^{3}H]CN-IMI	18.9	1.1
6	.81	$<10^{-3}$	[^{3}H]Paroxetine	13.6	0.9
7	.53	$<.01$	[^{3}H]Citalopram	5.0	4.9

Table 8:
Using age-corrected binding values for thalamus and striatal ROIs, linear regression models from SERT BP$_{ND}$ to B$_{max}$ (pmol/g tissue) were calculated for each autoradiography study separately. Midbrain and raphe ROIs were excluded from regression analyses. Model # refers to the respective *post mortem* study, as specified in Table 6.

Model #	ΔR^2	ΔF	p
1	.02 *	9.27	.01
2	.08 *	6.74	.04
3	.01	3.83	.08
4^a	0	0	.
5	.04 ***	69.57	$<10^{-3}$
6	.04 *	7.71	.02
7	.09	4.32	.06

Table 9:
Age correction of B$_{max}$ values of thalamus and striatal regions was performed to account for the different demography of subjects enrolled in *post mortem* studies. Improvement of all models affected can be seen as an increase of R^2 and F values. For 4 of the models this improvement was significant as shown by F-tests.

^{a} not affected by age correction
(*, p < 0.05; **, p < 0.01; ***, p < 0.001)
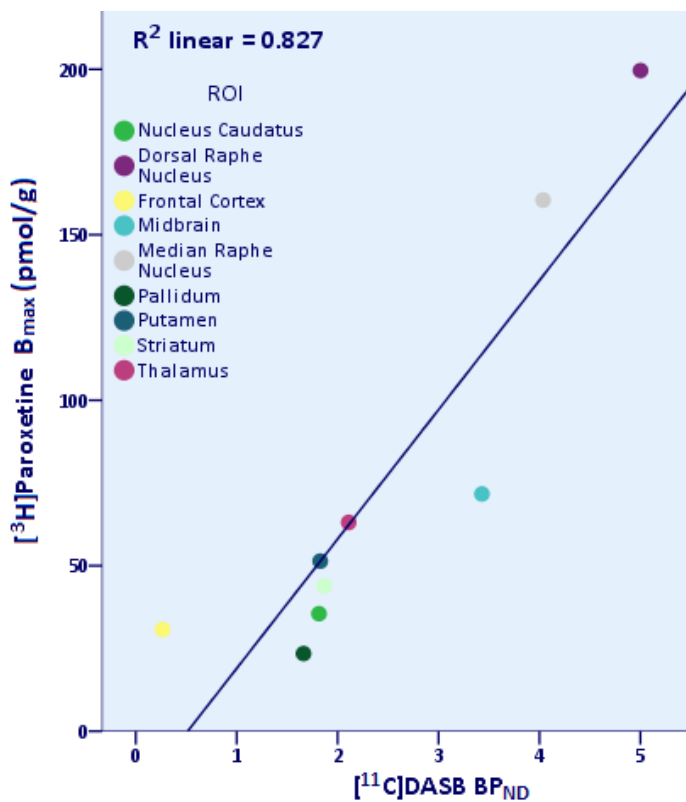
Figure 16:
Scatter plot showing correlation of mean SERT BP_{ND} and mean [³H]paroxetine B_{max} values (pmol/g tissue) adapted from Cortes et al (1988).

For information on how regions investigated in this autoradiography study were matched with PET ROIs see Table 11 and Table 13.

Correlation coefficients:
Pearson r: 0.91 $p < 10^{-3}$
Spearman ρ: 0.97 $p < 10^{-4}$

Figure 15:
Scatter plot showing correlation of mean SERT BP_{ND} and mean [³H]imipramine B_{max} values (pmol/g tissue) adapted from Gross-Isseroff and Biegon (1988).
For information on how regions investigated in this autoradiography study were matched with PET ROIs see Table 11 and Table 14.
(BA, Brodmann area)

Figure 17:
Scatter plots showing correlation of mean SERT BP$_{ND}$ and mean [^{3}H]citalopram B$_{max}$ values (pmol/g tissue) adapted from Chinaglia et al (1993). For information on how regions investigated in this autoradiography study were matched with PET ROIs see Table 11 and Table 15. Correlation coefficients:

Pearson r: 0.87   p < 10^{-3}
Spearman ρ: 0.92   p < 10^{-4}

R^2 values indicated a non-linear relationship between mean SERT binding potentials and absolute [^{3}H]citalopram binding, if all ROIs initially matched *post mortem – in vivo* were taken into account (left panel). This was supported by a F-test quadratic vs. linear regression model (ΔF = 13.4; p = 0.06). If midbrain and dorsal raphe nucleus were excluded, however, no significant advantage (ΔF = 0.10; p = 0.76) of non-linear over linear models could be seen (right panel).
(Ncl., Nucleus; BA, Brodmann area)

Figure 18:
Scatter plot showing correlation of mean SERT BP$_{ND}$ and mean [^{3}H]cyanoimipramine B$_{max}$ values (pmol/g tissue) adapted from Mann et al (2000).
Correlation coefficients:
Pearson r: 0.91   p = 0.08
Spearman ρ: 1   .
(BA, Brodmann area)

Figure 19:
Scatter plot showing correlation of mean SERT BP_{ND} and mean [³H]cyanoimipramine
B_{max} values (pmol/g tissue) adapted from Joyce et al (1993). For information on how regions investigated in this autoradiography study were matched with PET ROIs see Table 11 and Table 16.

Correlation coefficients:
Pearson r: 0.95 $p < 10^{-5}$
Spearman ρ: 0.75   p = 0.01
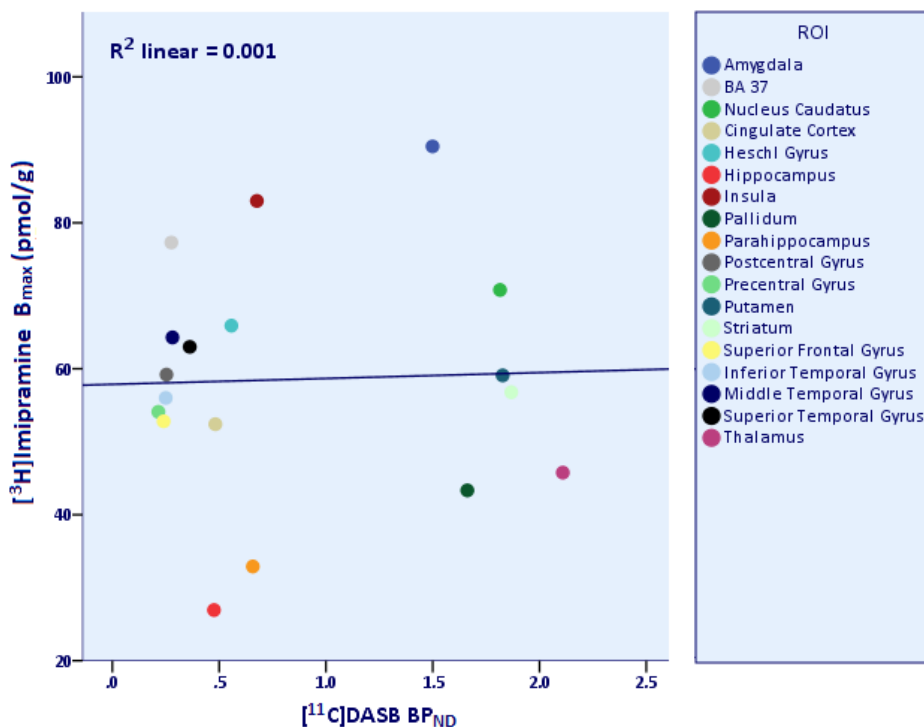**(Ncl., Nucleus; BA, Brodmann area)**
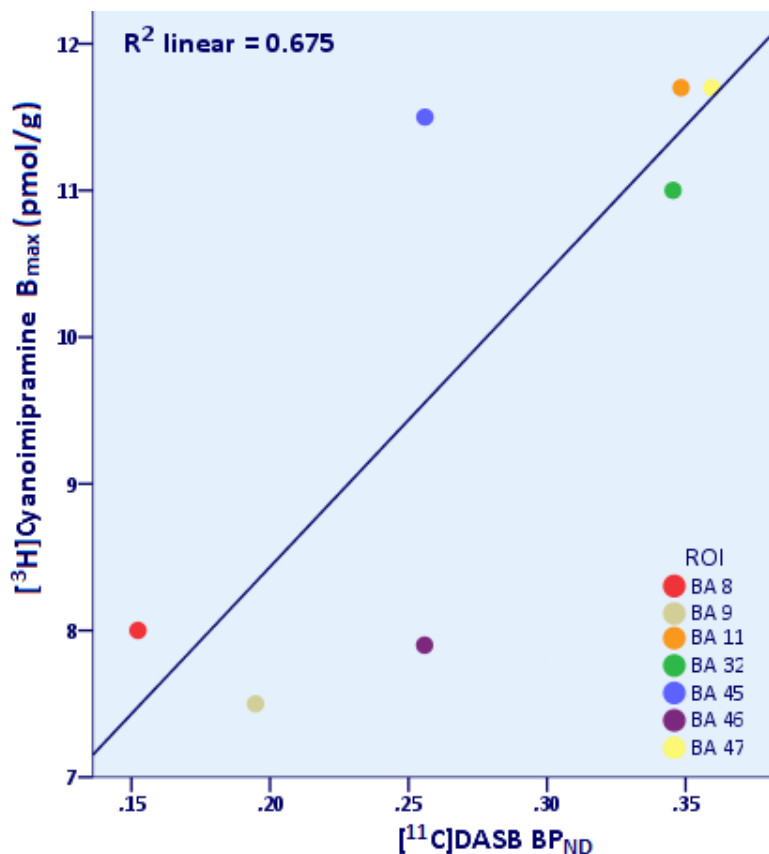
Figure 20:
Scatter plot of correlation of mean SERT BP_{ND} and mean [³H]cyanoimipramine
B_{max} values (pmol/g tissue) adapted from Arango et al (1995).

Correlation coefficients:
Pearson r: 0.82   p = 0.02
Spearman ρ: 0.85   p = 0.02
(BA, Brodmann area)
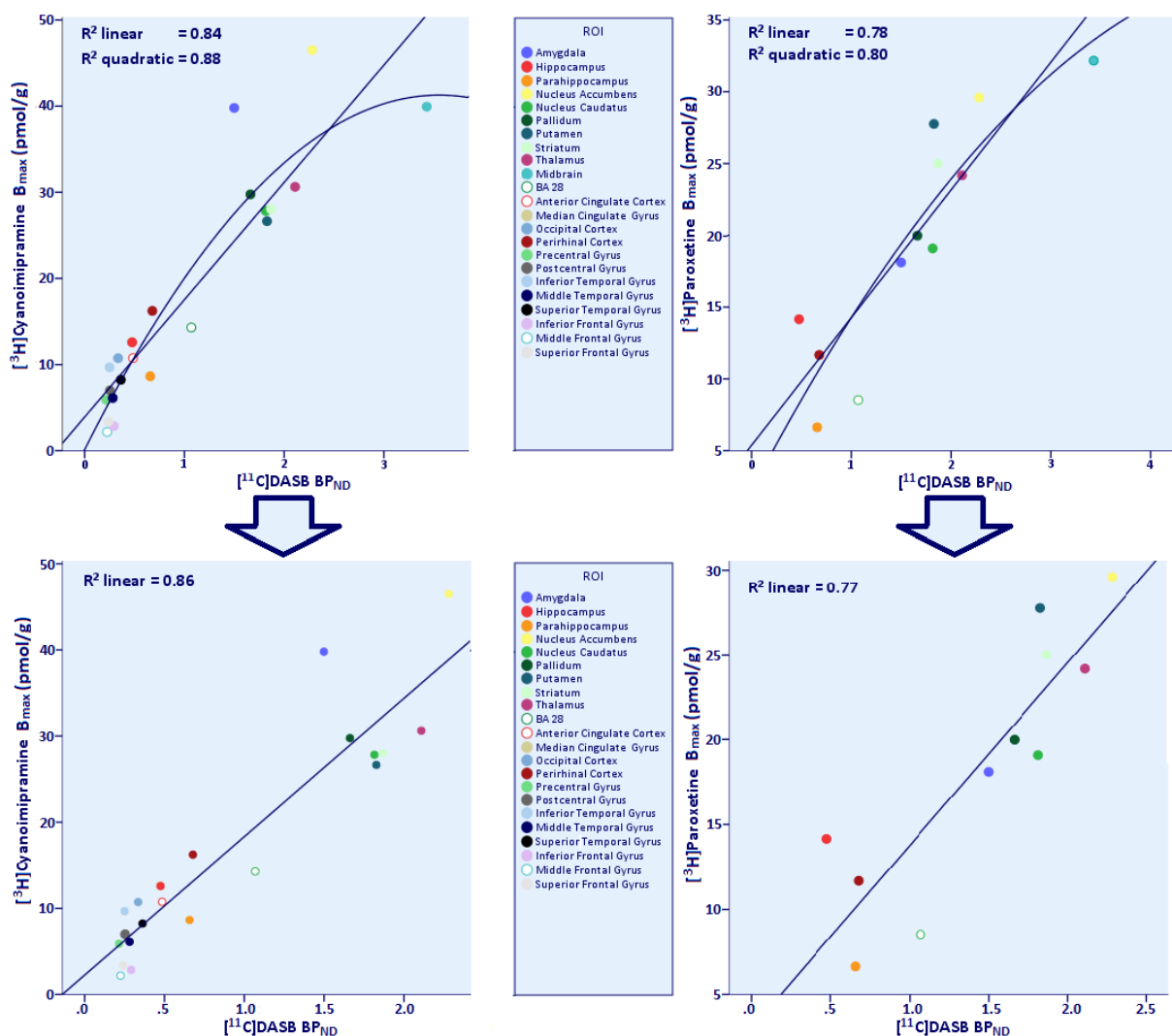
Figure 21:
Scatter plots showing correlation of mean SERT BP_{ND} and mean [³H]cyanoimipramine (upper left panel) and [³H]paroxetine (upper right panel) B_{max} values (pmol/g tissue) adapted from Gurevich and Joyce (1996).
For information on how regions investigated in this autoradiography study were matched with PET ROIs see Table 11 and Table 17.

Correlation coefficients:
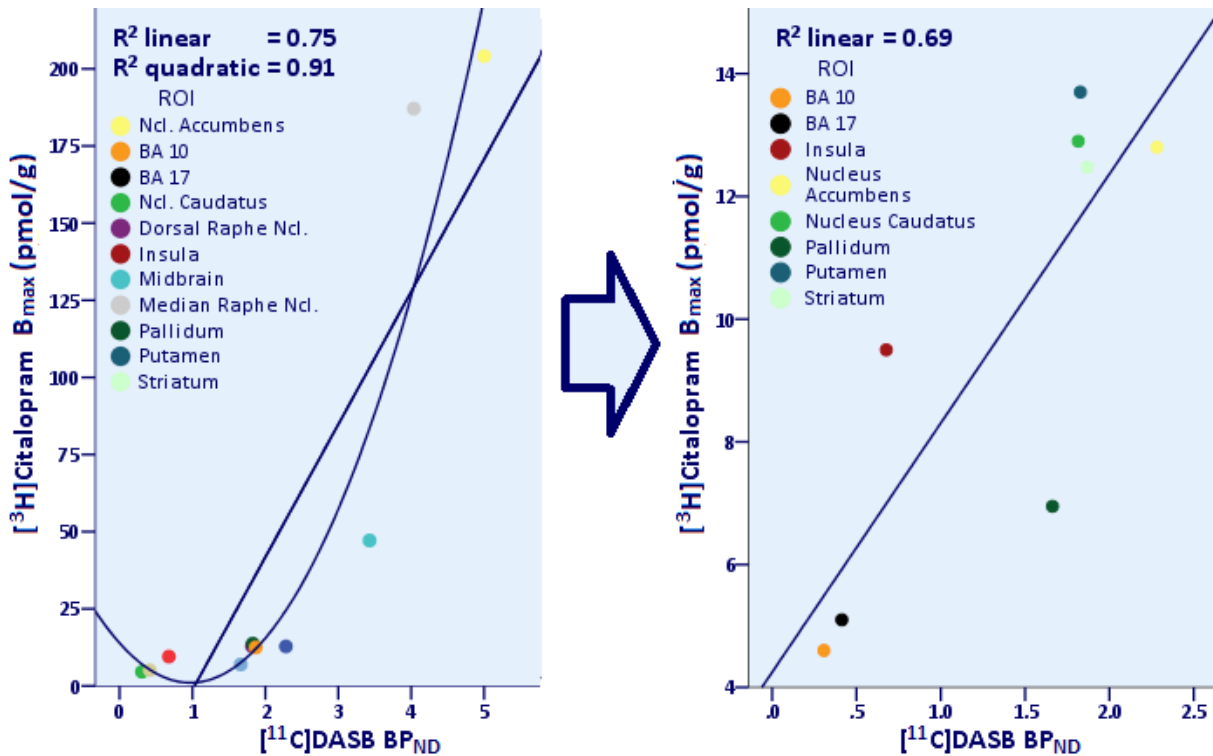[³H]Cyanoimipramine: Pearson r: 0.91 $p < 10^{-9}$ Spearman ρ: 0.92 $p < 10^{-9}$
[³H]Paroxetine: Pearson r: 0.89 $p < 10^{-3}$ Spearman ρ: 0.92 $p < 10^{-4}$

R^2 values indicated a non-linear relationship between mean SERT binding potentials and absolute [³H]cyanoimipramine binding, if all ROIs initially matched *post mortem - in vivo* were taken into account (upper left panel). This was supported by a significant F-test quadratic vs. linear regression model (ΔF = 6.9; p = 0.02). If the midbrain ROI was excluded, however, no significant advantage (ΔF = 0.001; p = 0.98) of non-linear over linear models could be seen (bottom left panel). The relationship between PET and [³H]paroxetine binding data was linear regardless of the inclusion of the midbrain in analyses.
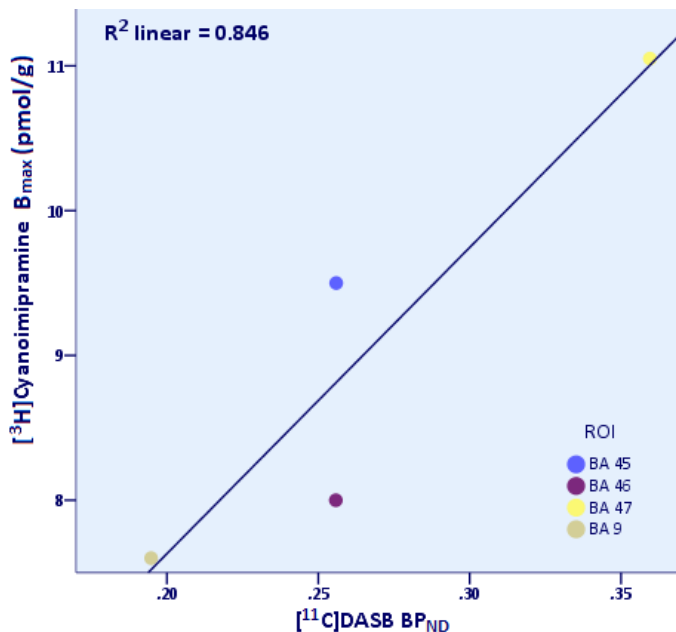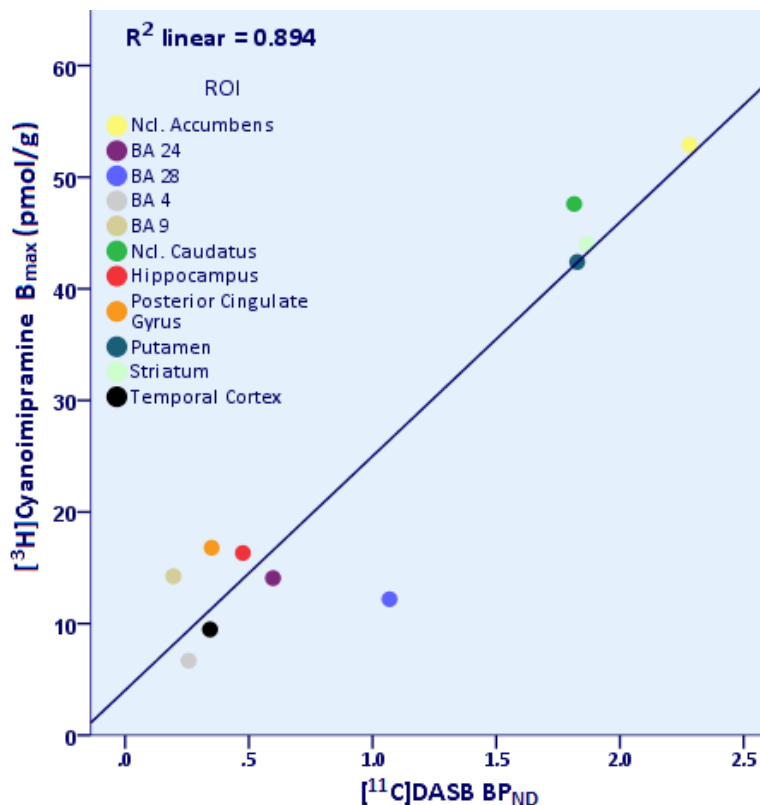(BA, Brodmann area)

47
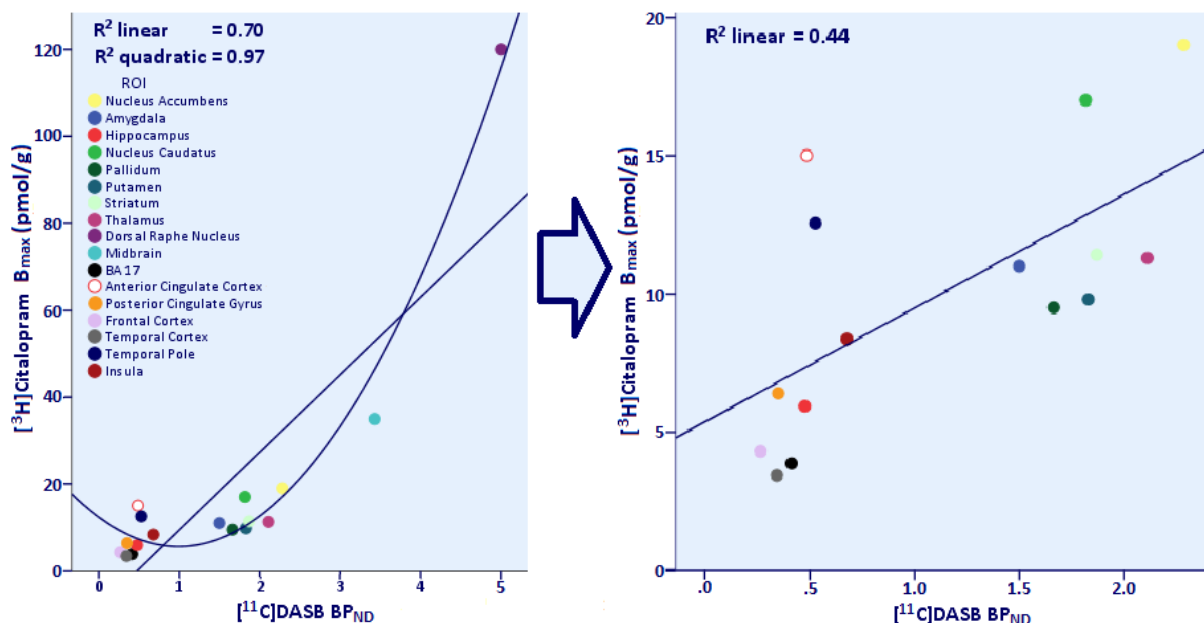
Figure 22:
Scatter plots showing correlation of mean SERT BP_{ND} and mean [³H]citalopram B_{max} values (pmol/g tissue) adapted from Varnäs et al (2004). For information on how regions investigated in this autoradiography study were matched with PET ROIs see Table 11 and Table 18.

Correlation coefficients:
Pearson r: **0.84**   **$p < 10^{-4}$**
Spearman ρ: **0.82**   **$p < 10^{-4}$**

R^2 values indicated a non-linear relationship between mean SERT binding potentials and absolute [³H]citalopram binding, if all ROIs initially matched *post mortem - in vivo* were taken into account (left panel). This was supported by a significant F-test quadratic vs. linear regression model ($\Delta F = 116.5$; $p < 10^{-7}$). If midbrain and dorsal raphe nucleus were excluded, however, no significant advantage ($\Delta F = 0.02$; $p = 0.89$) of non-linear over linear models could be seen (right panel).
(BA, Brodmann area)
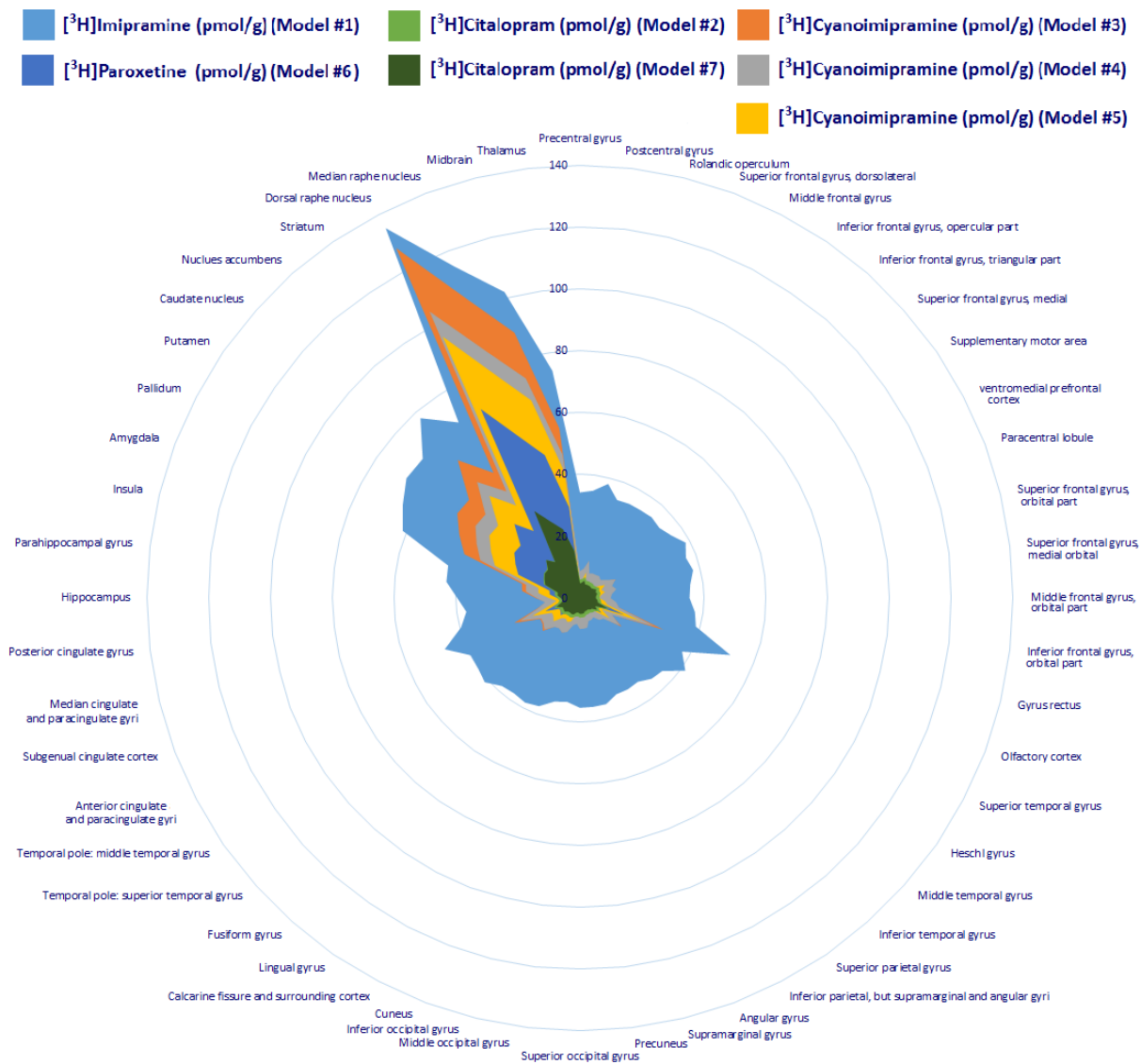
Figure 23:
Applying the linear equations listed in Table 8 to mean SERT BP$_{ND}$ values of AAL and subcortical ROI resulted in B$_{max}$ (pmol/g tissue) values for each ROI and model. A different colour was assigned to represent values calculated with each model.
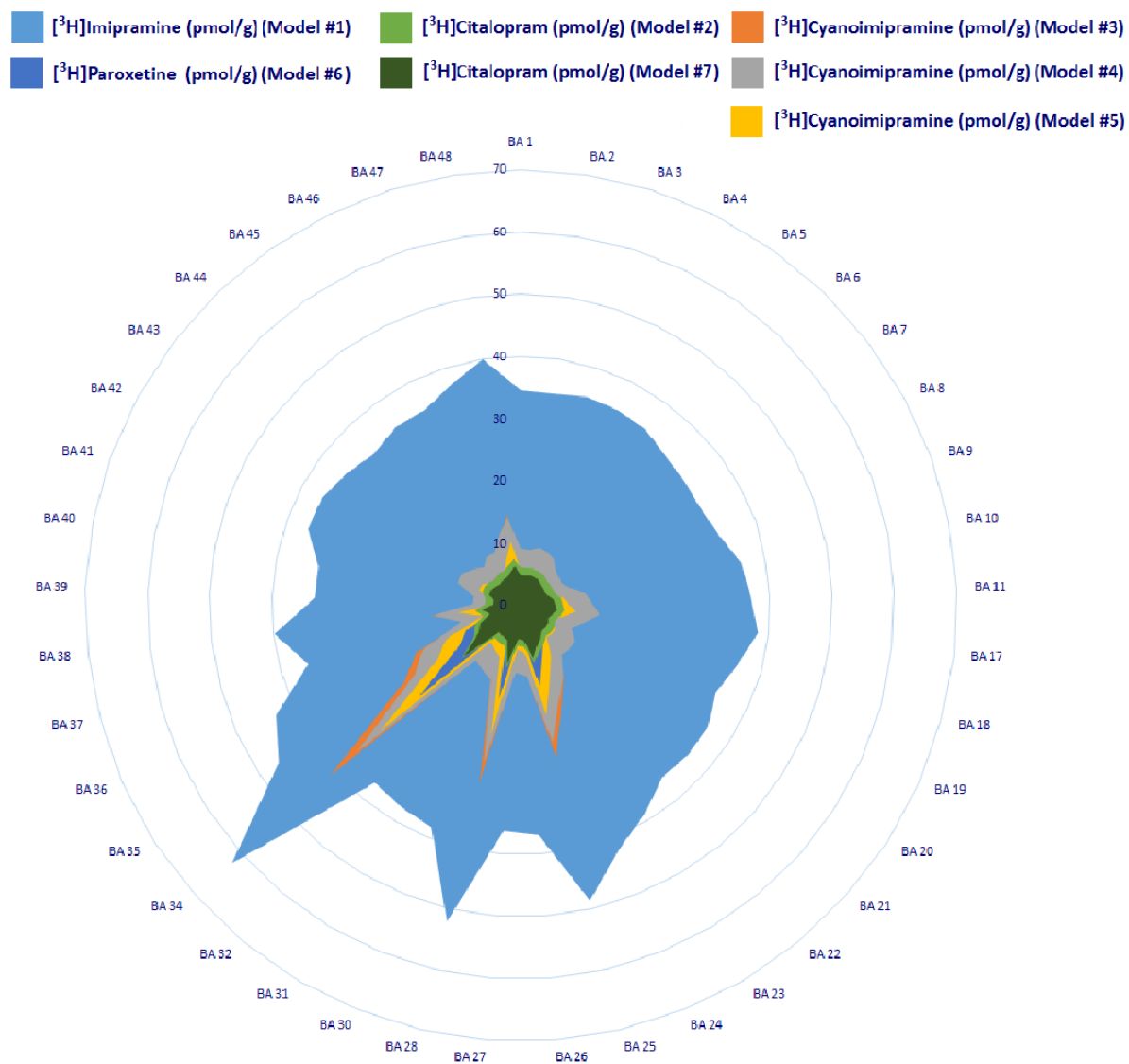
Figure 24:
Applying the linear equations listed in Table 8 to mean SERT BP$_{ND}$ values of Brodmann areas resulted in B$_{max}$ (pmol/g tissue) values for each BA and model. A different colour was assigned to represent values calculated with each model.

Despite their high significance, depending on the model used, calculated B$_{max}$ values vary substantially. This discrepancy is explained in the discussion section with the different methods used in autoradiography studies to determine binding densities.

7 DISCUSSION

7.1 Serotonin Transporter Binding Potential

SERT binding potential values assessed in the current investigation are in good agreement with most literature values on the distribution of SERT throughout the brain. [^{11}C]DASB PET along with automated calculation of BP_{ND} using the "multilinear reference tissue model" (MRTM/MRTM2) for standardized and broadly used ROIs (AAL and Brodmann areas) was already proven a valid method (Savli et al 2012). Savli et al (2012) determined SERT BP for a subgroup (n=18) of the study group in the current analysis and found it to correlate with values by other authors, derived using manual delineation methods, while eliminating the bias that can be ascribed to such procedures. The addition of 12 subjects did not alter obtained BP values substantially. The greatest deviations of BP_{ND} were found in the median raphe nucleus (+0.22), the midbrain ROI (+0.15), the thalamus (−0.07), the amygdala (−0.04) and the calcarine fissure and surrounding cortex ROI (+0.04).

Seeing such a small drift of values even in small ROIs known to possess the highest SERT densities confirms the reliability and quality of the method and reinforces the produced average values in the present sample as representative of a healthy Caucasian population.

7.2 Effects of Sex and Age

The effects of demographic variables on SERT, if present, are weak and require large samples to be unveiled.

In agreement with published *post mortem* and *in vivo* studies testing for the effects of sex on SERT, only slight tendencies towards lower SERT BP_{ND} in females were found which did not reach significance ($\alpha \leq 0.05$), even if no correction for multiple comparison was performed. Targeted testing in larger samples might reveal more.

Despite the fact that no significant effects of age on SERT BP were assessed, the tendencies seen were clearer than for the influence of sex. Decreasing BP in the thalamus is in agreement with published findings as discussed in the background section. The effect of age on other ROI BP found in the current investigation is a contrast to literature. Cortical regions were hardly appraised in this context so far, but a few *post mortem* studies reported an increase of SERT density with age, while in the current sample, SERT BP_{ND} tends to decrease in cortical ROIs. Similarly, most *in vivo* studies published agree on reporting a reduction of SERT in brainstem regions, whereas a SERT BP_{ND} increase in the dorsal raphe nucleus in the whole sample (n = 30) and in the median raphe nucleus of females (n = 11)was noted. Although none of these *in vivo* studies investigated the raphe nuclei specifically, assuming that the raphe nuclei account for a great part of brainstem SERT abundance, this is a striking result which should entail further appraisal. Another interesting circumstance observed was that, in spite of its smaller size, in the female sample the decline of BP was more pronounced in several regions. However, all of these results must be seen in the context of the limitations inherent in the method of SERT quantification via PET and [^{11}C]DASB: Due to low SERT densities in cortical regions, the low signal to noise ratio may account for a non-negligible part of the variance of BP_{ND} values in this part of the brain. At the same time the small size of the raphe nuclei leads to partial volume effects which in turn add to the variance of BP_{ND} assessed in this ROI among subjects.

Again, targeted testing in a larger (female) sample promises more distinct information.

7.3 Comparison with *Post Mortem* Data

Absolute regional SERT densities (B_{max}), measured within the scope of different autoradiography studies which constitute the gold standard of receptor and transporter quantification methods, excellently correlate with SERT binding potentials (BP_{ND}) obtained with PET using the highly selective tracer [^{11}C]DASB and automated ROI analysis. Thus, the validity of SERT quantification with [^{11}C]DASB applying standardized Brodmann area and AAL ROI templates and the MRTM/MRTM2 is once again confirmed.

Binding densities provided by 2 out of 10 autoradiography studies tested did not correlate significantly with binding potentials:

Values from Mann et al (2000) show a good association with BP despite the characterization of cortical regions where SERT quantification with PET could suffer from low signal to noise ratio. Unfortunately, only 4 ROIs could be compared yielding slightly insignificant p-values.

Gross-Isseroff and Biegon (1988) provided binding density values for plenty of regions, but these are not consistent with the state of knowledge on distribution of SERT throughout the brain. For example B_{max} values reported for thalamic and striatal regions, known for high SERT abundance, are in the same range as for parts of the cortex. No explanation for this discrepancy could be found.

7.3.1 REGRESSION ANALYSES

The regression from PET binding potentials to absolute SERT densities has already been performed by Savli et al (2012) for B_{max} values provided by Varnas et al (2004). Nevertheless, it was considered worthwhile to appraise the construability of these results in the context of a plethora of autoradiography studies which analysed SERT applying different methods.

7.3.1.1 Linearity

What immediately catches the eye of the investigator when comparing *post mortem* and *in vivo* data is the underestimation of SERT abundance in the raphe nuclei with PET. As discussed in the background section, PET imaging of small areas with high binding values surrounded by extensive areas with low binding, such as the raphe, suffers from low resolution of the method producing partial volume effects, a blending of neighbouring binding values.

Another region inconsistently fitting on the linear regression curves is the midbrain. In this case, the limitation of the current approach becomes apparent: The matching of ROIs *in vivo* to *post mortem* and vice versa was aimed at the inclusion of a large number of regions in order to increase the power of analyses. This, however, led to the pooling of binding density values of subregions of the midbrain which were not representative of the midbrain as a whole. For additional clarifications see the appendix section (page 64 ff.).

Since the inclusion of these ROIs bent the theoretically established linear relationship between absolute SERT density (B_{max}) and BP towards a non-linear one, the bias inherent in the reconciliation of binding values of these ROIs across methods warrants their exclusion in final regression analyses. This step successfully rendered non-linear regression models redundant, to the detriment of one model, connecting BP and [³H]paroxetine B_{max} values published by Cortes et al (1988), which lost significance due to the reduction in the number of ROIs.

7.3.1.2 Age Correction

Seeing no significant effects of age on SERT BP_{ND} in our own sample, the reasonableness of adjusting binding values to account for the differing demography of *post mortem* subjects had to be established separately. A rationale for age correction of thalamic, striatal and midbrain ROIs was derived from published literature (see Table 2). Since the midbrain was excluded in a previous step (see above), changes in models are merely attributable to age correction of thalamic and striatal binding values. All the more surprising is the significant improvement of most models afflicted by age correction, which might be interpreted as further support for the decline of SERT density in these regions with age.

7.3.1.3   Differences Between Models

Given the different methods applied by autoradiography studies, varying binding density values (B_{max}) are obtained leading to divergent linear equations connecting BP to B_{max}. The factor accounting for most of the variation among regression models is the radioligand used to bind SERT in each study. Therefore in the following section, studies using the same ligand will be discussed together.

Joyce et al (1993), Arango et al (1995) and Gurevich and Joyce (1996) labelled SERT with [³H]cyanoimipramine at a concentration of approximately $2*K_D$ in 20μm thick sections. This favourable methodical conformity lead to similar linear equations. A circumstance which might be responsible for a part of the discrepancy is the specification of B_{max} values in fmol/mg protein by Joyce et al (1993) and Gurevich and Joyce (1996), considering that the conversion factor from fmol/mg protein to pmol/g tissue is unlikely to be exactly 10 or equal for all brain regions and subjects. Furthermore, binding values published by Joyce et al (1993) and Arango et al (1995) were presented as graphs only compelling the use of a ruler to be read out.

A slightly higher conversion factor from SERT BP_{ND} to [³H]cyanoimipramine B_{max} values published by Joyce et al (1993) compared to the two other models was calculated. This can be accounted for by the use of desmethylimipramine to determine non-specific binding instead of citalopram or sertraline. Desmethylimipramine displays a higher affinity for the norepinephrine reuptake transporter (NET) than for SERT (Tatsumi et al 1997) and hence displaces [³H]cyanoimipramine from this target during the determination of non-specific binding. Thus, the small fraction of [³H]cyanoimipramine bound to NET is attributed to the ligands' specific binding. Another potential factor could be an overly rigorous age-correction of binding values, since a relatively large part of regions published by Joyce et al (1993) was affected.

Overall, quantification of SERT with [³H]cyanoimipramine as performed in these studies can be considered a reliable approach. For this reason and the high statistical significance of the regression model calculated with values published by Gurevich and Joyce (1996) for a plethora of regions measured in a large number of subjects, it was elected the preferred model for estimation of absolute SERT density (B_{max}) from PET SERT BP_{ND} data.

$$[^3H]Cyanoimipramine\ binding\ (pmol/g\ tissue) = 1.1 + 18.9 * [^{11}C]DASB\ BP_{ND}$$

Chinaglia et al (1993) and Varnas et al (2004) quantified SERT with [³H]citalopram at concentrations of approximately $1*K_D$ and $2*K_D$, respectively. The different ligands applied for the determination of non-specific binding should not alter results significantly, because both imipramine and fluoxetine, show good selectivity and high affinity for SERT. A potential confounding factor for the current analyses is that B_{max} was specified in different units in these two publications (fmol/mg protein vs. pmol/g tissue). Moreover, Varnas et al (2004) cut 100 μm thick sections, which necessitated correction for ³H-β-self-absorption. Notwithstanding a few outliers in terms of the agreement of BP and [³H]citalopram B_{max}, the models obtained for values from both studies are in very good agreement. However, the small number of subjects enrolled in these studies and the inability of these models to explain a large amount of the variance, as indicated by R^2 values, disqualify them for our inferential purposes in the presence of the [³H]cyanoimipramine models.

The model calculated with [³H]imipramine B_{max} values published by Cortes et al (1988) contains the highest conversion factor from BP to B_{max} and the highest constant value of all linear equations calculated. The latter prohibits the calculation of meaningful values for regions with low SERT densities, i.e. cortical ROIs. Cortes et al (1988) used high concentrations of radioligands ($\sim 7*K_D$) so that specific binding was similar to total binding density, but a non-negligible amount NET was bound ($\sim 0.3*K_D$) (Tatsumi et al 1997). Due to the determination of non-specific binding with desmethylimipramine, this bound NET fraction might have added noise to the measurement of SERT density, as explained above for data by Joyce et al (1993).

Lastly, the model for [³H]paroxetine B_{max} values by Gurevich and Joyce (1996) has a conversion factor which approximates the average of factors of [³H]cyanoimipramine and [³H]citalopram models. [³H]Paroxetine binding was measured in a smaller number of brain regions than [³H]cyanoimipramine binding, which is sufficient to explain the difference in significance of models calculated with this data. Since Gurevich and Joyce (1996) themselves found [³H]paroxetine binding to underestimate SERT density at high levels compared to [³H]cyanoimipramine, the model obtained with the latter is preferred.

7.4 Limitations

The ideal experiment to obtain valid equations for the calculation of absolute binding densities (B_{max}) from PET binding potentials would involve PET measurement and autoradiography of the same group of subjects with the same tracer together with a MR scan to align values in standardized MNI (Montreal Neurological Institute) or Talairach space.

The latter can be accomplished using *post mortem* material only by applying a MR scan before cryosectioning of brains. This would eliminate the confounding factor of matching regions assessed in autoradiography studies with PET ROIs arbitrarily based on nomenclature substantially increasing the power of regression analyses. Also feasible is the use of the same radioligand in PET and autoradiography to rule out tracer specific variations in binding across these methods.

PET measurement and autoradiography of the same subjects is difficult, if not impossible, to perform. The benefit over the current approach would be the possibility to compare BP and B_{max} values in the same brain regions for a number of patients, resulting in topologically specific regression models, which is statistically sounder than the comparison of mean values over all regions. Moreover, topological differences in the error of the PET quantification method could be revealed.

Lastly, what cannot be ruled out when comparing binding densities from autoradiographic analyses and PET data are changes in conformation, distribution, availability between the *in vivo* and *post mortem* conditions.

7.5 Conclusion

Post mortem studies have long been the only means of receptor and transporter molecules quantification in human brains. They currently still constitute the gold standard of absolute quantification methods, fostering the expansion of *in vivo* molecular imaging methods which make attractive study designs possible in order to answer questions raised in many fields of neuroscience.

The current investigation showed by the example of the serotonin reuptake transporter that receptor or transporter quantification methods with PET can profit from autoradiographic analyses by extracting conversion formulas to estimate absolute receptor or transporter availability. This approach not only validates PET measurements, but allows for the comparison of absolute densities of different structures imaged *in vivo*, which in turn makes the development of complex multi-receptor and –transporter models possible. These could be used to topologically predict alterations in brain functionality assessed, for example, by functional magnetic resonance imaging elicited by the application of psychiatric drugs such as SSRIs.

On the other hand, the comparison of PET and *post mortem* data is useful to identify regions in which binding is not accurately assessed with PET BP, e.g. due to partial volume effects, such as the raphe nuclei in the case of SERT BP. Starting from there, correction factors for the *in vivo* imaging of such regions could be calculated.

Future studies quantifying a broad range of structures using PET and autoradiography with the same tracer molecules aligning measures to standardized brain coordinate systems are essential to consolidate the applicability of this promising method.

8 APPENDIX

8.1 SERT Binding Potential Table

Table 10:
Mean (n = 30), minimal (min.) and maximal (max.) SERT binding potentials (BP_{ND}), standard deviation (SD), volumes and binding density (B_{max}) of 52 ROIs defined by the AAL parcellation scheme plus subcortical regions and of 41 Brodmann areas. BPs of cortical ROIs were averaged over the left and right hemispheres.
B_{max} is given in pmol/g tissue and was calculated using the Model #5 obtained using age-corrected [³H]cyanoimipramine binding density values from Gurevich and Joyce (1996).

[a] Values below zero are may be calculated in regions with negligible amounts of SERT.

(AAL, Automated Anatomical Labelling; BP, binding potential; SD, standard deviation; min., minimal BP values; max., maximal BP values; B_{max}, absolute binding densities calculated using mean BP values and Model #5; BA, Brodmann area)

Region of interest (AAL)	Volume (cm³)	BP_{mean}	SD	Min.	Max.	B_{max} (pmol/g)
Total binding	941.90	.36	.07	.24	.50	7.86
Subcortical regions						
Amygdala	3.56	1.50	.25	1.03	2.17	29.37
Pallidum	1.46	1.66	.22	1.26	2.19	32.45
Putamen	5.90	1.83	.23	1.32	2.23	35.57
Caudate nucleus	1.76	1.82	.25	1.35	2.37	35.34
Nuclues accumbens	0.33	2.28	.40	1.58	3.12	44.14
Striatum	9.86	1.87	.23	1.37	2.25	36.34
Dorsal raphe nucleus	0.05	5.00	1.02	3.23	7.81	95.47
Median raphe nucleus	0.05	4.04	1.08	2.80	6.77	77.25
Midbrain	0.70	3.43	.58	2.59	4.88	65.81
Thalamus	4.60	2.11	.26	1.65	2.75	40.89
Central region						
Precentral gyrus	37.01	.22	.10	.02	.44	5.15
Postcentral gyrus	40.73	.25	.10	.07	.44	5.87
Rolandic operculum	13.70	.40	.10	.23	.62	8.60
Frontal lobe, lateral surface						
Superior frontal gyrus, dorsolateral	54.88	.20	.08	.06	.36	4.90
Middle frontal gyrus	58.30	.22	.07	.09	.36	5.33
Inferior frontal gyrus, opercular part	15.49	.23	.08	.10	.40	5.46
Inferior frontal gyrus, triangular part	15.28	.25	.08	.12	.42	5.82

Frontal lobe, medial surface	Volume (cm³)	BP$_{mean}$	SD	Min.	Max.	B$_{max}$ (pmol/g)
Superior frontal gyrus, medial	42.06	.22	.08	.05	.40	5.24
Supplementary motor area	36.68	.29	.09	.12	.50	6.57
Ventromedial prefrontal cortex	32.11	.42	.09	.28	.59	9.09
Paracentral lobule	12.87	.33	.11	.15	.57	7.36
Frontal lobe, orbital surface						
Superior frontal gyrus, orbital part	14.28	.38	.08	.24	.51	8.30
Superior frontal gyrus, medial orbital	15.38	.30	.07	.18	.43	6.71
Middle frontal gyrus, orbital part	13.38	.28	.07	.14	.40	6.28
Inferior frontal gyrus, orbital part	19.58	.37	.10	.22	.59	8.08
Gyrus rectus	8.85	.43	.10	.24	.62	9.13
Olfactory cortex	3.58	1.06	.21	.70	1.59	21.09
Temporal lobe, lateral surface						
Superior temporal gyrus	31.20	.36	.09	.21	.53	7.93
Heschl gyrus	3.23	.56	.13	.31	.82	11.60
Middle temporal gyrus	47.92	.28	.07	.12	.39	6.40
Inferior temporal gyrus	39.13	.25	.06	.13	.39	5.81
Parietal lobe, lateral surface						
Superior parietal gyrus	33.27	.16	.08	−.02[a]	.29	4.06
Inferior parietal, but supramarginal and angular gyri	26.42	.18	.06	.04	.28	4.41
Angular gyrus	19.78	.17	.06	.04	.28	4.36
Supramarginal gyrus	13.50	.27	.08	.12	.42	6.21
Parietal lobe, medial surface						
Precuneus	48.86	.28	.09	.07	.44	6.31
Occipital lobe, lateral surface						
Superior occipital gyrus	13.06	.28	.08	.01	.41	6.35
Middle occipital gyrus	22.45	.20	.06	.01	.30	4.88
Inferior occipital gyrus	9.47	.23	.08	.04	.41	5.44
Occipital lobe, medial and inferior surfaces						
Cuneus	14.73	.37	.11	.02	.60	8.04
Calcarine fissure and surrounding cortex	13.66	.41	.13	.00	.62	8.75
Lingual gyrus	25.55	.37	.11	.08	.64	8.12
Fusiform gyrus	35.94	.40	.08	.22	.59	8.60

Limbic lobe	(cm³)	BP$_{mean}$	SD	Min.	Max.	B$_{max}$ (pmol/g)
Temporal pole: superior temporal gyrus	18.78	.54	.11	.26	.73	11.36
Temporal pole: middle temporal gyrus	10.05	.49	.11	.29	.72	10.40
Anterior cingulate and paracingulate gyri	13.51	.49	.09	.31	.62	10.25
Subgenual cingulate cortex	1.42	.81	.18	.56	1.41	16.43
Median cingulate and paracingulate gyri	15.91	.47	.09	.34	.64	10.01
Posterior cingulate gyrus	2.75	.35	.11	.12	.57	7.68
Hippocampus	5.30	.48	.13	.29	.74	10.07
Parahippocampal gyrus	12.99	.66	.13	.41	.88	13.50
Insula						
Insula	32.77	.68	.11	.51	.91	13.86

Brodmann areas	(cm³)	BP$_{mean}$	SD	Min.	Max.	B$_{max}$ (pmol/g)
BA 1	2.37	.24	.11	.01	.43	5.53
BA 2	11.47	.23	.09	.05	.39	5.40
BA 3	17.11	.26	.10	.06	.48	6.06
BA 4	30.31	.26	.11	.03	.50	5.92
BA 5	18.84	.24	.10	.08	.44	5.60
BA 6	76.66	.18	.08	.03	.36	4.52
BA 7	51.33	.16	.08	−.02 [a]	.29	4.11
BA 8	25.80	.15	.08	.00	.34	3.96
BA 9	35.93	.19	.08	.03	.34	4.76
BA 10	39.82	.31	.08	.15	.46	6.88
BA 11	40.90	.35	.08	.22	.49	7.66
BA 17	21.55	.41	.13	.03	.63	8.89
BA 18	52.74	.31	.10	.03	.48	6.87
BA 19	49.54	.22	.07	.01	.35	5.26
BA 20	59.91	.29	.07	.14	.44	6.64
BA 21	28.41	.30	.07	.17	.44	6.79
BA 22	14.25	.29	.08	.15	.44	6.58
BA 23	11.07	.44	.09	.25	.62	9.43
BA 24	9.46	.60	.11	.40	.82	12.37
BA 25	5.53	.90	.19	.59	1.48	18.16
BA 26	0.70	.35	.11	.13	.56	7.64
BA 27	1.89	.32	.13	.10	.72	7.05
BA 28	3.66	1.07	.19	.60	1.53	21.26
BA 30	11.57	.42	.09	.26	.59	8.97

Brodmann areas	(cm³)	BP, mean	SD	Min.	Max.	B_max (pmol/g)
BA 31	18.08	.38	.09	.18	.54	8.28
BA 32	28.60	.35	.08	.19	.47	7.61
BA 34	3.42	1.54	.26	1.03	2.22	30.22
BA 35	4.10	.79	.18	.34	1.11	16.02
BA 36	12.02	.64	.11	.45	.82	13.16
BA 37	47.74	.28	.07	.09	.43	6.30
BA 38	20.47	.48	.12	.16	.69	10.24
BA 39	25.18	.17	.06	.02	.27	4.23
BA 40	28.95	.16	.07	.02	.27	4.17
BA 41	2.88	.32	.09	.19	.50	7.11
BA 42	6.10	.32	.09	.18	.51	7.07
BA 43	4.55	.26	.09	.07	.43	5.99
BA 44	14.90	.20	.08	.06	.38	4.95
BA 45	19.29	.26	.08	.14	.42	5.92
BA 46	24.18	.26	.07	.15	.39	5.91
BA 47	23.03	.36	.09	.22	.57	7.87
BA 48	101.46	.49	.09	.34	.68	10.41

8.2 Fitting ROIs *In Vivo* to *Post Mortem*

The following table shows how AAL and Brodmann Area ROIs were pooled to fit larger regions characterized in autoradiography studies.

New ROI	BP	Volume (cm³)	Parts (sub-ROIs)
Frontal cortex	.27	347.63	Precentral gyrus; superior & inferior frontal gyrus; middle frontal gyrus; middle frontal gyrus, orbital part; supplementary motor area; rolandic operculum; paracentral lobule; gyrus rectus; olfactory cortex
Parietal cortex	.22	141.83	Superior parietal gyrus; inferior parietal, but supramarginal and angular gyri; angular gyrus; supramarginal gyrus; precuneus
Temporal cortex	.34	150.31	Superior, middle & inferior temporal gyrus; Heschl gyrus; temporal pole
Occipital cortex	.33	134.87	Superior, middle & inferior occipital gyrus; cuneus; calcarine fissure and surrounding cortex; lingual & fusiform gyri
Cingular cortex	.48	33.60	Anterior, posterior, median & para -cingulate gyri; subgenual cingulate cortex
Superior frontal gyrus	.24	126.60	Superior frontal gyrus: medial, orbital, medial orbital & dorsolateral part
Inferior frontal gyrus	.29	50.35	Inferior frontal gyrus: opercular, triangular & orbital part
Temporal pole	.53	28.83	temporal pole: superior & middle temporal gyrus
Perirhinal Cortex	.68	16.11	BA 35; BA 36
Entorhinal Cortex	1.07	3.66	BA 28

Table 11:
The regions listed in the first column were characterized in *post mortem* studies and had to be matched with appropriate *in vivo* ROIs. Therefore "new ROI" binding potentials were calculated using ROI SERT BP values listed in Table 10.
First, the BP of each part (sub-ROI) was multiplied by its volume; results were summed; and then divided by the volume of the new ROI to obtain new BPs.

(BP, calculated binding potential used in analyses)

8.3 Fitting ROIs *Post Mortem* to *In Vivo*

In this section it is shown, how regions and binding densities characterized in *post mortem* studies are adjusted to fit AAL and Brodmann area ROIs. Since most studies did not use standardized parcellation schemes, different techniques had to be used for many regions to accomplish this goal. Therefore, on the following pages, there is one paragraph for each autoradiography study clarifying the methods used to match regions with *in vivo* ROIs. In most cases, simple arithmetic mean calculations sufficed. For several regions, binding of a sub-region was used to represent B_{max} (pars pro toto). Finally, for a few regions, binding density was calculated correcting for the volume of their parts (Table 12). To obtain B_{max} pmol/g tissue, B_{max} values given in pmol/g protein were divided by 10 according to estimates of chemical composition of brain tissue (Ericsson et al 2007, Swatton et al 2004).

ROI	Parts (volume factor)
Hippocampus	Dentate gyrus (1); cornu ammonis fields (2)
Amygdala[a]	Basal nucleus (2); basal accessory nucleus (1); lateral nucleus (3); corticomedial complex (2); other parts (1 each)
Striatum[b]	Pallidum; putamen; nucleus caudatus; nucleus accumbens; substantia innominata (striatal minus other ROI volumes)
Midbrain[c]	Midbrain regions (87); dorsal raphe nucleus (2)
Thalamus[d]	Median nuclei (0.5 each); anterior nucleus (1); pulvinar (5); nucleus medials dorsalis (5); other parts (1 each)

Table 12:
Given the different volume of sub-regions for the ROIs listed in the first column, an attempt was made to correct for the contribution of each part to the binding density of the whole ROI. This was accomplished by multiplying the B_{max} of each part by a volume factor, adding the results, and dividing this sum by the sum of volume factors of parts included in the first step of the calculation.

[a] Volume factors were estimated using published *post mortem* measures of amygdala sub-nuclei volumes (Harding et al 2002, Schumann & Amaral 2006).
[b] Volume factors were adapted from PET ROI volumes listed in Table 10.
[c] Midbrain and dorsal raphe nucleus ROIs share 2 voxels.
[d] Volume factors were estimated using published *post mortem* measures of thalamic sub-nuclei volumes (Byne et al 2002, Danos et al 2003).

8.3.1 CORTES ET AL (1988)

ROI	B_{max} (pmol/g)	Adjustments made
Hippocampus	44.38	Volume corrected[a] binding density was calculated using B_{max} values of dentate gyrus and cornu ammonis 1 & 3.
Parahippocampal gyrus	48.05	Subiculum (pars pro toto).
Amygdala	47.37	Volume corrected[a] binding density was calculated using B_{max} values of basal, basal accessory, lateral, and granular nucleus.
Pallidum	60.84	Average of globus pallidus and substantia innominata binding.
Striatum	59.65	Volume corrected[a] binding density was calculated using B_{max} values of nucleus caudatus, pallidum, globus plallidus lateralis, and substantia innominata.
Dorsal raphe nucleus	237.81	Average of B_{max} values measured at different levels.
Median raphe nucleus	154.95	Average of B_{max} values measured at different levels.
Midbrain	106.41	Volume corrected[a] binding density was calculated using B_{max} values of central gray, substantia nigra, and red, interpeduncular, tegmental pendunculo-pontine and dorsal raphe nucleus.
Thalamus	67.91	Volume corrected[a] binding density was calculated using B_{max} values of the zona incerta, and anterior, anterolateral, medial, paramedian rotundocellular and reuniens nucleus.

Table 13:
Methods used to match regions used by Cortes et al (1988) to PET ROIs.
Resulting [³H]imipramine B_{max} (pmol/g tissue) values are listed.

[a] See Table 12.
(B_{max}, calculated absolute SERT density used in analyses)

8.3.2 GROSS-ISSEROFF AND BIEGON (1988)

ROI	B_{max} (pmol/g)	Adjustments made
Hippocampus	26.93	Volume corrected[a] binding density was calculated using B_{max} values of dentate gyrus (hilus, molecular-, and granular layer) and cornu ammonis parts (molecular-, and pyramidal layer).
Parahippocampal gyrus	32.90	Average of parahippocampal gyrus and subiculum binding.
Amygdala	90.47	Volume corrected[a] binding density was calculated using B_{max} values of basal, basal accessory, lateral, central, cortical, and medial nucleus.
Pallidum	43.33	Average of lateral & medial globus pallidus, and substantia innominata binding.
Nucleus caudatus	70.80	Head and body (pars pro toto).
Striatum	56.79	Volume corrected[a] binding density was calculated using B_{max} values of putamen, nucleus caudatus, globus pallidus, and substantia innominata.
Thalamus	45.76	Volume corrected[a] binding density was calculated using B_{max} values of the anterior, ventrolateral and medial nucleus.
BA 37	77.30	Lateral occipitotemporal gyrus binding was used.

Table 14:
Methods used to match regions used by Gross-Isseroff and Biegon (1988) to PET ROIs.
Resulting [³H]imipramine B_{max} (pmol/g tissue) values are listed.

[a] See Table 11.
(B_{max}, calculated absolute SERT density used in analyses)

8.3.3 CHINAGLIA ET AL (1993)

ROI	B_{max} (pmol/g)	Adjustments made
Pallidum	6.95	Average of lateral & medial globus pallidus binding.
Nucleus caudatus	12.90	Average of ventral and dorsal nucleus caudaus head binding.
Striatum	12.47	Volume corrected[a] binding density was calculated using B_{max} values of putamen, globus pallidus, nucleus caudatus, and -accumbens.
Midbrain	47.14	Volume corrected[a] binding density was calculated using B_{max} values of substantia nigra and dorsal raphe nucleus.

Table 15:
Methods used to match regions used by Chinaglia et al (1993) to PET ROIs. Resulting [³H]citalopram B_{max} (pmol/g tissue) values are listed.

[a] See Table 12.
(B_{max}, calculated absolute SERT density used in analyses)

8.3.4 JOYCE ET AL (1993)

B_{max} values for different layers in cortical regions are provided in this study. These values were averaged for each cortical region. For subcortical regions, several simple adjustments were made Table 16.

ROI	B_{max} (pmol/g)	Adjustments made
Hippocampus	16.79	Volume corrected[a] binding density was calculated using B_{max} values of dentate gyrus (granular layer) and cornu ammonis 1 & 3.
Putamen	42.40	Dorsal putamen (pars pro toto).
Nucleus caudatus	47.60	Dorsal nucleus caudatus (pars pro toto).
Striatum	43.97	Volume corrected[a] binding density was calculated using B_{max} values of putamen, nucleus caudatus and -accumbens.

Table 16:
Methods used to match regions used by to PET ROIs.
Resulting [³H]cyanoimipramine B_{max} (pmol/g tissue) values are listed.

[a] See Table 12.
(B_{max}, calculated absolute SERT density used in analyses)

8.3.5 ARANGO ET AL (1995)

Arango et al (1995) used the classical cytoarchitectonic Brodmann (1909) parcellation scheme. Therefore, no adjustments had to be made.

8.3.6 MANN ET AL (2000)

This study divided several Brodmann Areas into sulcal and gyral sub-regions. Binding densities of these were averaged to obtain B_{max} for BA.

8.3.7 GUREVICH AND JOYCE (1996)

ROI	B_{max} (pmol/g)	Adjustments made
Precentral gyrus	5.90	Average of precentral gyrus (superior, middle & inferior frontal gyrus) binding.
Postcentral gyrus	6.99	Average of postcentral gyrus (superior, middle & inferior frontal gyrus) binding.
Middle frontal gyrus	2.18	Prefrontal Cortex, middle frontal gyrus binding was used.
Anterior cingulate and paracingulate gyri	10.75	Prefrontal Cortex, cingulate gyrus binding was used.
Median cingulate and paracingulate gyri	12.63	Average of precentral gyrus (cingulate gyrus) and postcentral gyrus (cingulate gyrus) binding.
Hippocampus	12.58	Volume corrected[a] binding density was calculated using B_{max} values of stratum lacunosum moleculare, dentate gyrus (molecular & granular layer) and cornu ammonis 1-3.
Parahippocampal gyrus	8.64	Average of subiculum, pre- & parasubiculum binding.
Amygdala	39.79	Volume corrected[a] binding density was calculated using B_{max} values of the anterior amygdaloid area and the basomedial, basolateral, mediodorsal, lateral, vertical cortical, and central nucleus.
Pallidum	29.76	Average of lateral & medial globus pallidus binding.
Putamen	26.64	Average of putamen (caudal striatum) and ventral & dorsal putamen (rostral striatum) binding.
Nucleus caudatus	27.83	Average of caudatum (caudal striatum) and ventral & dorsal caudatum (rostral striatum) binding.
Striatum	28.03	Volume corrected[a] binding density was calculated using B_{max} values of putamen, pallidum, nucleus caudatus and -accumbens.
Midbrain	39.94	Average of central gray, substantia nigra (pars reticulata, compacta & lateralis), red, parabrachial pigmented and paranigral nucleus binding.
Thalamus	30.62	Volume corrected[a] binding density was calculated using B_{max} values of zona incerta, and the anteroventral, mediodorsal, centromedian, parafascicular, posterolateral and ventral posterolateral nucleus.

Table 17:
Methods used to match regions used by Gurevich and Joyce (1996) to PET ROIs.
Resulting [³H]Cyanoimipramine B_{max} (pmol/g tissue) values are listed.

[a] See Table 12.
(B_{max}, calculated absolute SERT density used in analyses)

8.3.8 VARNAS ET AL (2004)

Varnas et al (2004) listed B_{max} values for different layers in cortical regions. These values were averaged for each cortical region. For subcortical regions, several simple adjustments were made (Table 18).

ROI	B_{max} (pmol/g)	Adjustments made
Hippocampus	5.93	Binding densities of dentate gyrus and the cornu ammonis fields (pyramidal & molecular layer) were averaged.
Amygdala	11.00	Nucleus basolateralis (pars pro toto)
Pallidum	9.50	Ventral pallidum and globus pallidus binding were averaged.
Nucleus accumbens	19.00	Ventral striatum binding was used.
Striatum	11.41	Volume corrected[a] binding density was calculated using B_{max} values of putamen, globus pallidus, nucleus caudatus, and -accumbens.
Midbrain	34.95	Volume corrected[a] binding density was calculated using B_{max} values of dorsal raphe nucleus, substantia nigra and central gray.
Thalamus	11.29	Volume corrected[a] binding density was calculated using B_{max} values of pulvinar, mediodorsal, and anterior nucleus.

Table 18:
Methods used to match regions used by Varnas et al (2004) to PET ROIs.
Resulting [³H]Citalopram B_{max} (pmol/g tissue) values are listed.

[a] See Table 12.
(B_{max}, calculated absolute SERT density used in analyses)

9 ABBREVIATIONS

[^{123}I]ADAM	[^{123}I] 2-((2-((dimethylamino)methyl) phenyl)thio)-5-iodophenylamine
[^{123}I]β-CIT	[^{123}I]-Methyl (1R,2S,3S)-3-(4-iodophenyl)-8-methyl-8-azabicyclo[3.2.1]octane-2-carboxylate
[^{11}C]DASB	[^{11}C]-N,N-dimethyl-2-(2-amino-4-cyanophenylthio)-benzylamine
[^{11}C]MADAM	[^{11}C]-N,N-dimethyl-2-(2-amino-4-methylphenylthio)-benzylamine
[^{11}C]McN5652	[^{11}C]-(+)-6beta-(4-Methylthiophenyl)-1,2,3,5,6 α,10 β-hexahydropyrrolo[2,1-a]isoquinoline
5-HT	Serotonin
ADHD	Attention Deficit Hyperactivity Disorder
AAL	Automated Anatomical Labelling
BA	Brodmann area
B	Number of bound target molecules
B/F	Quotient of bound and free ligand
B_{avail}	Number of free target molecules, ready to be bound
BP	Binding potential
B_{max}	Maximal binding density
C	Concentration
DA	Dopamine
DAT	Dopamine reuptake transporter
DSM-IV	Diagnostic and Statistical Manual of Mental Disorders, Fourth Edition
e^- / e^+	Electron / positron
GCP	Good clinical practice
EK	Ethik-Kommission
fMRI	functional magnetic resonance imaging
FWHM	Full width at half-maximum
HCG	Human chorionic gonadotropin
K_D	Dissociation constant
k_{OFF}	Dissociation rate constant
k_{ON}	Association rate constant
LOR	Line of response
MAT	Monoamine transporter
MDD	Major depressive disorder
MRI	Magnetic resonance imaging
NE	Norepinephrine
NET	Norepinephrine reuptake transporter
PET	Positron emission tomography
ROI	Region of interest
SCID	Structured Clinical Interview for DSM Disorders
SD	Standard deviation
SERT	Serotonin reuptake transporter
SLC 6	Solute carrier family 6
NRI	Norepinephrine reuptake inhibitor
SPECT	Single-photon emission computed tomography
SSRI	Selective serotonin reuptake inhibitor
THC	Tetrahydrocannabinol

10 REFERENCES

Abrams TE, Lund BC, Bernardy NC, Friedman MJ. 2013. Aligning clinical practice to PTSD treatment guidelines: medication prescribing by provider type. *Psychiatric services* 64: 142-8

Agam G, Everall IP, Belmaker RH. 2002. *The Postmortem Brain in Psychiatric Research*. Springer.

Agnati LF, Zoli M, Stromberg I, Fuxe K. 1995. Intercellular communication in the brain: wiring versus volume transmission. *Neuroscience* 69: 711-26

Akimova E, Lanzenberger R, Kasper S. 2009. The Serotonin-1A Receptor in Anxiety Disorders. *Biol Psychiatry* 66: 627-35

Amara SG, Kuhar MJ. 1993. Neurotransmitter transporters: recent progress. *Annual review of neuroscience* 16: 73-93

Andersson A, Sundman I, Marcusson J. 1992. Age stability of human brain 5-HT terminals studied with [3H]paroxetine binding. *Gerontology* 38: 127-32

Arakawa R, Okumura M, Ito H, Seki C, Takahashi H, et al. 2008. Quantitative analysis of norepinephrine transporter in the human brain using PET with (S,S)-18F-FMeNER-D2. *J Nucl Med* 49: 1270-6

Arango V, Underwood MD, Gubbi AV, Mann JJ. 1995. Localized alterations in pre- and postsynaptic serotonin binding sites in the ventrolateral prefrontal cortex of suicide victims. *Brain research* 688: 121-33

Arranz B, Eriksson A, Mellerup E, Plenge P, Marcusson J. 1993. Effect of aging in human cortical pre- and postsynaptic serotonin binding sites. *Brain research* 620: 163-6

Aston-Jones G, Cohen JD. 2005. An integrative theory of locus coeruleus-norepinephrine function: adaptive gain and optimal performance. *Annual review of neuroscience* 28: 403-50

Bailey DL. 2005. *Positron Emission Tomography: Basic Sciences*. Springer.

Benarroch EE. 2009. The locus ceruleus norepinephrine system: functional organization and potential clinical significance. *Neurology* 73: 1699-704

Berger MJ, Seltzer SM, Aeronautics USN, Administration S, Standards USNBo. 1964. *Tables of Energy Losses and Ranges of Electrons and Positrons*. Scientific and Technical Information Division, National Aeronautics and Space Administration.

Berridge CW, Waterhouse BD. 2003. The locus coeruleus-noradrenergic system: modulation of behavioral state and state-dependent cognitive processes. *Brain research. Brain research reviews* 42: 33-84

Biederman J, Spencer T. 1999. Attention-deficit/hyperactivity disorder (ADHD) as a noradrenergic disorder. *Biol Psychiatry* 46: 1234-42

Bjorklund A, Dunnett SB. 2007. Dopamine neuron systems in the brain: an update. *Trends in neurosciences* 30: 194-202

Bligh-Glover W, Kolli TN, Shapiro-Kulnane L, Dilley GE, Friedman L, et al. 2000. The serotonin transporter in the midbrain of suicide victims with major depression. *Biol Psychiatry* 47: 1015-24

Bonisch H, Bruss M. 2006. The norepinephrine transporter in physiology and disease. *Handbook of experimental pharmacology*: 485-524

Borgkvist A, Malmlof T, Feltmann K, Lindskog M, Schilstrom B. 2012. Dopamine in the hippocampus is cleared by the norepinephrine transporter. *Int J Neuropsychopharmacol* 15: 531-40

Borowsky B, Hoffman BJ. 1995. Neurotransmitter transporters: molecular biology, function, and regulation. *International review of neurobiology* 38: 139-99

Brodmann K. 1909. Beschreibung der einzelnen Hirnkarten.

Bunin MA, Wightman RM. 1998. Quantitative evaluation of 5-hydroxytryptamine (serotonin) neuronal release and uptake: an investigation of extrasynaptic transmission. *The Journal of neuroscience : the official journal of the Society for Neuroscience* 18: 4854-60

Bunin MA, Wightman RM. 1999. Paracrine neurotransmission in the CNS: involvement of 5-HT. *Trends in neurosciences* 22: 377-82

Bymaster FP, Katner JS, Nelson DL, Hemrick-Luecke SK, Threlkeld PG, et al. 2002. Atomoxetine increases extracellular levels of norepinephrine and dopamine in prefrontal cortex of rat: a potential mechanism for efficacy in attention deficit/hyperactivity disorder. *Neuropsychopharmacology : official publication of the American College of Neuropsychopharmacology* 27: 699-711

Byne W, Buchsbaum MS, Mattiace LA, Hazlett EA, Kemether E, et al. 2002. Postmortem assessment of thalamic nuclear volumes in subjects with schizophrenia. *Am J Psychiatry* 159: 59-65

Cannon DM, Ichise M, Fromm SJ, Nugent AC, Rollis D, et al. 2006. Serotonin transporter binding in bipolar disorder assessed using [11C]DASB and positron emission tomography. *Biol Psychiatry* 60: 207-17

Carboni E, Silvagni A. 2004. Dopamine reuptake by norepinephrine neurons: exception or rule? *Critical reviews in neurobiology* 16: 121-8

Carboni E, Silvagni A, Vacca C, Di Chiara G. 2006. Cumulative effect of norepinephrine and dopamine carrier blockade on extracellular dopamine increase in the nucleus accumbens shell, bed nucleus of stria terminalis and prefrontal cortex. *Journal of neurochemistry* 96: 473-81

Carboni E, Spielewoy C, Vacca C, Nosten-Bertrand M, Giros B, Di Chiara G. 2001. Cocaine and amphetamine increase extracellular dopamine in the nucleus accumbens of mice lacking the dopamine transporter gene. *The Journal of neuroscience : the official journal of the Society for Neuroscience* 21: RC141: 1-4

Carboni E, Tanda GL, Frau R, Di Chiara G. 1990. Blockade of the noradrenaline carrier increases extracellular dopamine concentrations in the prefrontal cortex: evidence that dopamine is taken up in vivo by noradrenergic terminals. *Journal of neurochemistry* 55: 1067-70

Caro LG, Van Tubergen RP, Kolb JA. 1962. High-resolution autoradiography. I. Methods. *The Journal of cell biology* 15: 173-88

Castelli MP, Mocci I, Langlois X, Gommerendagger W, Luyten WH, et al. 2000. Quantitative autoradiographic distribution of gamma-hydroxybutyric acid binding sites in human and monkey brain. *Brain research. Molecular brain research* 78: 91-9

Chalon S, Tarkiainen J, Garreau L, Hall H, Emond P, et al. 2003. Pharmacological characterization of N,N-dimethyl-2-(2-amino-4-methylphenyl thio)benzylamine as a ligand of the serotonin transporter with high affinity and selectivity. *The Journal of pharmacology and experimental therapeutics* 304: 81-7

Chen F, Lawrence AJ. 2003. The effects of antidepressant treatment on serotonergic and dopaminergic systems in Fawn-Hooded rats: a quantitative autoradiography study. *Brain research* 976: 22-9

Chinaglia G, Alvarez FJ, Probst A, Palacios JM. 1992. Mesostriatal and mesolimbic dopamine uptake binding sites are reduced in Parkinson's disease and progressive supranuclear palsy: a quantitative autoradiographic study using [3H]mazindol. *Neuroscience* 49: 317-27

Chinaglia G, Landwehrmeyer B, Probst A, Palacios JM. 1993. Serotoninergic terminal transporters are differentially affected in Parkinson's disease and progressive supranuclear palsy: an autoradiographic study with [3H]citalopram. *Neuroscience* 54: 691-9

Cortes R, Soriano E, Pazos A, Probst A, Palacios JM. 1988. Autoradiography of antidepressant binding sites in the human brain: localization using [3H]imipramine and [3H]paroxetine. *Neuroscience* 27: 473-96

Danos P, Baumann B, Krämer A, Bernstein H-G, Stauch R, et al. 2003. Volumes of association thalamic nuclei in schizophrenia: a postmortem study. *Schizophrenia research* 60: 141-55

Daws LC. 2009. Unfaithful neurotransmitter transporters: focus on serotonin uptake and implications for antidepressant efficacy. *Pharmacology & therapeutics* 121: 89-99

Dean B, Tomaskovic-Crook E, Opeskin K, Keks N, Copolov D. 1999. No change in the density of the serotonin1A receptor, the serotonin4 receptor or the serotonin transporter in the dorsolateral prefrontal cortex from subjects with schizophrenia. *Neurochemistry international* 34: 109-15

Devauges V, Sara SJ. 1990. Activation of the noradrenergic system facilitates an attentional shift in the rat. *Behavioural brain research* 39: 19-28

Emond P, Garreau L, Chalon S, Boazi M, Caillet M, et al. 1997. Synthesis and ligand binding of nortropane derivatives: N-substituted 2beta-carbomethoxy-3beta-(4'-iodophenyl)nortropane and N-(3-iodoprop-(2E)-enyl)-2beta-carbomethoxy-3beta-(3',4'-disubstituted phenyl)nortropane. New high-affinity and selective compounds for the dopamine transporter. *Journal of medicinal chemistry* 40: 1366-72

Ericsson C, Peredo I, Nister M. 2007. Optimized protein extraction from cryopreserved brain tissue samples. *Acta Oncol* 46: 10-20

Erritzoe D, Frokjaer VG, Haahr MT, Kalbitzer J, Svarer C, et al. 2010. Cerebral serotonin transporter binding is inversely related to body mass index. *Neuroimage* 52: 284-9

Eshleman AJ, Carmolli M, Cumbay M, Martens CR, Neve KA, Janowsky A. 1999. Characteristics of drug interactions with recombinant biogenic amine transporters expressed in the same cell type. *The Journal of pharmacology and experimental therapeutics* 289: 877-85

Flaherty AW. 2005. Frontotemporal and dopaminergic control of idea generation and creative drive. *The Journal of comparative neurology* 493: 147-53

Franco-Perez J, Ballesteros-Zebadua P, Custodio V, Paz C. 2012. [Major neurotransmitters involved in the regulation of sleep-wake cycle]. *Revista de investigacion clinica; organo del Hospital de Enfermedades de la Nutricion* 64: 182-91

Frankle WG, Huang Y, Hwang D-R, Talbot PS, Slifstein M, et al. 2004. Comparative Evaluation of Serotonin Transporter Radioligands 11C-DASB and 11C-McN 5652 in Healthy Humans. *Journal of Nuclear Medicine* 45: 682-94

Frankle WG, Narendran R, Huang Y, Hwang DR, Lombardo I, et al. 2005. Serotonin transporter availability in patients with schizophrenia: a positron emission tomography imaging study with [11C]DASB. *Biol Psychiatry* 57: 1510-6

Garris PA, Ciolkowski EL, Pastore P, Wightman RM. 1994. Efflux of dopamine from the synaptic cleft in the nucleus accumbens of the rat brain. *The Journal of neuroscience : the official journal of the Society for Neuroscience* 14: 6084-93

Ginovart N, Wilson AA, Meyer JH, Hussey D, Houle S. 2001. Positron emission tomography quantification of [(11)C]-DASB binding to the human serotonin transporter: modeling strategies. *J Cereb Blood Flow Metab* 21: 1342-53

Giros B, el Mestikawy S, Godinot N, Zheng K, Han H, et al. 1992. Cloning, pharmacological characterization, and chromosome assignment of the human dopamine transporter. *Molecular pharmacology* 42: 383-90

Giros B, Wang YM, Suter S, McLeskey SB, Pifl C, Caron MG. 1994. Delineation of discrete domains for substrate, cocaine, and tricyclic antidepressant interactions using chimeric dopamine-norepinephrine transporters. *The Journal of biological chemistry* 269: 15985-8

Gonzalez AM, Berciano J, Figols J, Pazos A, Pascual J. 2000. Loss of dopamine uptake sites and dopamine D2 receptors in striatonigral degeneration. *Brain research* 852: 228-32

Gross-Isseroff R, Biegon A. 1988. Autoradiographic analysis of [3H]imipramine binding in the human brain postmortem: effects of age and alcohol. *Journal of neurochemistry* 51: 528-34

Gu H, Wall SC, Rudnick G. 1994. Stable expression of biogenic amine transporters reveals differences in inhibitor sensitivity, kinetics, and ion dependence. *The Journal of biological chemistry* 269: 7124-30

Gu HH, Wall S, Rudnick G. 1996. Ion coupling stoichiometry for the norepinephrine transporter in membrane vesicles from stably transfected cells. *The Journal of biological chemistry* 271: 6911-6

Gulyas B, Brockschnieder D, Nag S, Pavlova E, Kasa P, et al. 2010. The norepinephrine transporter (NET) radioligand (S,S)-[18F]FMeNER-D2 shows significant decreases in NET density in the human brain in Alzheimer's disease: a post-mortem autoradiographic study. *Neurochemistry international* 56: 789-98

Gurevich EV, Joyce JN. 1996. Comparison of [3H]paroxetine and [3H]cyanoimipramine for quantitative measurement of serotonin transporter sites in human brain. *Neuropsychopharmacology : official publication of the American College of Neuropsychopharmacology* 14: 309-23

Haeusler D, Mien LK, Nics L, Ungersboeck J, Philippe C, et al. 2009. Simple and rapid preparation of [11C]DASB with high quality and reliability for routine applications. *Appl Radiat Isot* 67: 1654-60

Haleem DJ. 1993. Serotonergic neurotransmission in the regulation of appetite: a receptor approach. *Pakistan journal of pharmaceutical sciences* 6: 89-96

Halldin C, Lundberg J, Sovago J, Gulyas B, Guilloteau D, et al. 2005. [(11)C]MADAM, a new serotonin transporter radioligand characterized in the monkey brain by PET. *Synapse* 58: 173-83

Harding AJ, Stimson E, Henderson JM, Halliday GM. 2002. Clinical correlates of selective pathology in the amygdala of patients with Parkinson's disease. *Brain* 125: 2431-45

Heinz A, Ragan P, Jones DW, Hommer D, Williams W, et al. 1998. Reduced central serotonin transporters in alcoholism. *Am J Psychiatry* 155: 1544-9

Heiss WD, Herholz K. 2006. Brain receptor imaging. *J Nucl Med* 47: 302-12

Hertting G, Axelrod J. 1961. Fate of tritiated noradrenaline at the sympathetic nerve-endings. *Nature* 192: 172-3

Hesse S, Barthel H, Murai T, Muller U, Muller D, et al. 2003. Is correction for age necessary in neuroimaging studies of the central serotonin transporter? *Eur J Nucl Med Mol Imaging* 30: 427-30

Ho PS, Ho KK, Huang WS, Yen CH, Shih MC, et al. 2012. Association study of serotonin transporter availability and SLC6A4 gene polymorphisms in patients with major depression. *Psychiatry research*

Hornung JP. 2003. The human raphe nuclei and the serotonergic system. *Journal of chemical neuroanatomy* 26: 331-43

Houle S, Ginovart N, Hussey D, Meyer JH, Wilson AA. 2000. Imaging the serotonin transporter with positron emission tomography: initial human studies with [11C]DAPP and [11C]DASB. *European journal of nuclear medicine* 27: 1719-22

Huang J, Pickel VM. 2002. Serotonin transporters (SERTs) within the rat nucleus of the solitary tract: subcellular distribution and relation to 5HT2A receptors. *Journal of neurocytology* 31: 667-79

Ichimiya T, Suhara T, Sudo Y, Okubo Y, Nakayama K, et al. 2002. Serotonin transporter binding in patients with mood disorders: a PET study with [11C](+)McN5652. *Biol Psychiatry* 51: 715-22

Ichise M, Liow JS, Lu JQ, Takano A, Model K, et al. 2003. Linearized reference tissue parametric imaging methods: application to [11C]DASB positron emission tomography studies of the serotonin transporter in human brain. *J Cereb Blood Flow Metab* 23: 1096-112

Innis RB, Cunningham VJ, Delforge J, Fujita M, Gjedde A, et al. 2007. Consensus nomenclature for in vivo imaging of reversibly binding radioligands. *J Cereb Blood Flow Metab* 27: 1533-9

Ito H, Takahashi H, Arakawa R, Takano H, Suhara T. 2008. Normal database of dopaminergic neurotransmission system in human brain measured by positron emission tomography. *Neuroimage* 39: 555-65

Iversen LL. 1971. Role of transmitter uptake mechanisms in synaptic neurotransmission. *British journal of pharmacology* 41: 571-91

Jacobsen LK, Staley JK, Malison RT, Zoghbi SS, Seibyl JP, et al. 2000. Elevated central serotonin transporter binding availability in acutely abstinent cocaine-dependent patients. *Am J Psychiatry* 157: 1134-40

Jayanthi LD, Ramamoorthy S. 2005. Regulation of monoamine transporters: influence of psychostimulants and therapeutic antidepressants. *The AAPS journal* 7: E728-38

Jodal L, Le Loirec C, Champion C. 2012. Positron range in PET imaging: an alternative approach for assessing and correcting the blurring. *Physics in medicine and biology* 57: 3931-43

Jovanovic H, Lundberg J, Karlsson P, Cerin A, Saijo T, et al. 2008. Sex differences in the serotonin 1A receptor and serotonin transporter binding in the human brain measured by PET. *Neuroimage* 39: 1408-19

Joyce JN, Shane A, Lexow N, Winokur A, Casanova MF, Kleinman JE. 1993. Serotonin uptake sites and serotonin receptors are altered in the limbic system of schizophrenics. *Neuropsychopharmacology : official publication of the American College of Neuropsychopharmacology* 8: 315-36

Kalbitzer J, Frokjaer VG, Erritzoe D, Svarer C, Cumming P, et al. 2009. The personality trait openness is related to cerebral 5-HTT levels. *Neuroimage* 45: 280-5

Kent L, Doerry U, Hardy E, Parmar R, Gingell K, et al. 2002. Evidence that variation at the serotonin transporter gene influences susceptibility to attention deficit hyperactivity disorder (ADHD): analysis and pooled analysis. *Mol Psychiatry* 7: 908-12

Kish SJ, Furukawa Y, Chang LJ, Tong J, Ginovart N, et al. 2005. Regional distribution of serotonin transporter protein in postmortem human brain: is the cerebellum a SERT-free brain region? *Nuclear medicine and biology* 32: 123-8

Klimek V, Roberson G, Stockmeier CA, Ordway GA. 2003. Serotonin transporter and MAO-B levels in monoamine nuclei of the human brainstem are normal in major depression. *J Psychiatr Res* 37: 387-97

Klimek V, Stockmeier C, Overholser J, Meltzer HY, Kalka S, et al. 1997. Reduced levels of norepinephrine transporters in the locus coeruleus in major depression. *The Journal of neuroscience : the official journal of the Society for Neuroscience* 17: 8451-8

Korr H, Bauer K, Bunzeck A-S, Nacken M, Karbach FT. 1997. Correction factors of 3H-β-self-absorption for quantitative autoradiography of different cell types in the brain of pre- and postnatal mice. *Histochemistry* 108: 537-41

Kovachich GB, Aronson CE, Brunswick DJ, Frazer A. 1988. Quantitative autoradiography of serotonin uptake sites in rat brain using [3H]cyanoimipramine. *Brain research* 454: 78-88

Kranz GS, Kasper S, Lanzenberger R. 2010. Reward and the serotonergic system. *Neuroscience* 166: 1023-35

Kumar S, Ranjan P, Mittal B, Ghoshal UC. 2012. Serotonin transporter gene (SLC6A4) polymorphism in patients with irritable bowel syndrome and healthy controls. *Journal of gastrointestinal and liver diseases : JGLD* 21: 31-8

Kung HF. 1991. Overview of radiopharmaceuticals for diagnosis of central nervous disorders. *Critical reviews in clinical laboratory sciences* 28: 269-86

Lanzenberger R, Kranz GS, Haeusler D, Akimova E, Savli M, et al. 2012. Prediction of SSRI treatment response in major depression based on serotonin transporter interplay between median raphe nucleus and projection areas. *Neuroimage* 63: 874-81

Lanzenberger RR, Mitterhauser M, Spindelegger C, Wadsak W, Klein N, et al. 2007. Reduced Serotonin-1A Receptor Binding in Social Anxiety Disorder. *Biol Psychiatry* 61: 1081-89

Larsen AK, Brennum LT, Egebjerg J, Sanchez C, Halldin C, Andersen PH. 2004. Selectivity of (3)H-MADAM binding to 5-hydroxytryptamine transporters in vitro and in vivo in mice; correlation with behavioural effects. *British journal of pharmacology* 141: 1015-23

Lawrence KM, De Paermentier F, Lowther S, Crompton MR, Katona CL, Horton RW. 1997. Brain 5-hydroxytryptamine uptake sites labeled with [3H]paroxetine in antidepressant drug-treated depressed suicide victims and controls. *Journal of psychiatry & neuroscience : JPN* 22: 185-91

Lawrence KM, Kanagasundaram M, Lowther S, Katona CL, Crompton MR, Horton RW. 1998. [3H] imipramine binding in brain samples from depressed suicides and controls: 5-HT uptake sites compared with sites defined by desmethylimipramine. *Journal of affective disorders* 47: 105-12

Layer RT, Uretsky NJ, Wallace LJ. 1992. Effect of serotonergic agonists in the nucleus accumbens on d-amphetamine-stimulated locomotion. *Life Sci* 50: 813-20

Li W, Yang Y, Lin J, Wang S, Zhao J, et al. 2013. Association of serotonin transporter gene (SLC6A4) polymorphisms with schizophrenia susceptibility and symptoms in a Chinese-Han population. *Prog Neuropsychopharmacol Biol Psychiatry* 44: 290-5

Little KY, Kirkman JA, Carroll FI, Clark TB, Duncan GE. 1993. Cocaine use increases [3H]WIN 35428 binding sites in human striatum. *Brain research* 628: 17-25

Little KY, McLaughlin DP, Zhang L, McFinton PR, Dalack GW, et al. 1998. Brain dopamine transporter messenger RNA and binding sites in cocaine users: a postmortem study. *Archives of general psychiatry* 55: 793-9

Little KY, McLauglin DP, Ranc J, Gilmore J, Lopez JF, et al. 1997. Serotonin transporter binding sites and mRNA levels in depressed persons committing suicide. *Biol Psychiatry* 41: 1156-64

Logan J, Wang GJ, Telang F, Fowler JS, Alexoff D, et al. 2007. Imaging the norepinephrine transporter in humans with (S,S)-[11C]O-methyl reboxetine and PET: problems and progress. *Nuclear medicine and biology* 34: 667-79

Lundberg J, Halldin C, Farde L. 2006. Measurement of serotonin transporter binding with PET and [11C]MADAM: a test-retest reproducibility study. *Synapse* 60: 256-63

Lundberg J, Odano I, Olsson H, Halldin C, Farde L. 2005. Quantification of 11C-MADAM binding to the serotonin transporter in the human brain. *J Nucl Med* 46: 1505-15

Mann JJ, Huang YY, Underwood MD, Kassir SA, Oppenheim S, et al. 2000. A serotonin transporter gene promoter polymorphism (5-HTTLPR) and prefrontal cortical binding in major depression and suicide. *Archives of general psychiatry* 57: 729-38

Mantere T, Tupala E, Hall H, Sarkioja T, Rasanen P, et al. 2002. Serotonin transporter distribution and density in the cerebral cortex of alcoholic and nonalcoholic comparison subjects: a whole-hemisphere autoradiography study. *Am J Psychiatry* 159: 599-606

McElroy SL, Guerdjikova AI, Mori N, O'Melia AM. 2012. Current pharmacotherapy options for bulimia nervosa and binge eating disorder. *Expert opinion on pharmacotherapy* 13: 2015-26

Meyer JH, Houle S, Sagrati S, Carella A, Hussey DF, et al. 2004. Brain serotonin transporter binding potential measured with carbon 11-labeled DASB positron emission tomography: effects of major depressive episodes and severity of dysfunctional attitudes. *Archives of general psychiatry* 61: 1271-9

Meyer JH, Wilson AA, Ginovart N, Goulding V, Hussey D, et al. 2001. Occupancy of serotonin transporters by paroxetine and citalopram during treatment of depression: a [(11)C]DASB PET imaging study. *Am J Psychiatry* 158: 1843-9

Miner LH, Schroeter S, Blakely RD, Sesack SR. 2003. Ultrastructural localization of the norepinephrine transporter in superficial and deep layers of the rat prelimbic prefrontal cortex and its spatial relationship to probable dopamine terminals. *The Journal of comparative neurology* 466: 478-94

Mintun MA, Raichle ME, Kilbourn MR, Wooten GF, Welch MJ. 1984. A quantitative model for the in vivo assessment of drug binding sites with positron emission tomography. *Annals of neurology* 15: 217-27

Moron JA, Brockington A, Wise RA, Rocha BA, Hope BT. 2002. Dopamine uptake through the norepinephrine transporter in brain regions with low levels of the dopamine transporter: evidence from knock-out mouse lines. *The Journal of neuroscience : the official journal of the Society for Neuroscience* 22: 389-95

Moses WW. 2011. Fundamental limits of spatial resolution in PET. *Nuclear Instruments and Methods in Physics Research Section A: Accelerators, Spectrometers, Detectors and Associated Equipment* 648, Supplement 1: S236-S40

Mossner R, Simantov R, Marx A, Lesch KP, Seif I. 2006. Aberrant accumulation of serotonin in dopaminergic neurons. *Neuroscience letters* 401: 49-54

Moya PR, Wendland JR, Rubenstein LM, Timpano KR, Heiman GA, et al. 2013. Common and rare alleles of the serotonin transporter gene, SLC6A4, associated with Tourette's disorder. *Movement disorders : official journal of the Movement Disorder Society*

Newberg AB, Amsterdam JD, Wintering N, Ploessl K, Swanson RL, et al. 2005. 123I-ADAM binding to serotonin transporters in patients with major depression and healthy controls: a preliminary study. *J Nucl Med* 46: 973-7

Nirenberg MJ, Chan J, Pohorille A, Vaughan RA, Uhl GR, et al. 1997. The dopamine transporter: comparative ultrastructure of dopaminergic axons in limbic and motor compartments of the nucleus accumbens. *The Journal of neuroscience : the official journal of the Society for Neuroscience* 17: 6899-907

Nirenberg MJ, Vaughan RA, Uhl GR, Kuhar MJ, Pickel VM. 1996. The dopamine transporter is localized to dendritic and axonal plasma membranes of nigrostriatal dopaminergic neurons. *The Journal of neuroscience : the official journal of the Society for Neuroscience* 16: 436-47

Ogden RT, Ojha A, Erlandsson K, Oquendo MA, Mann JJ, Parsey RV. 2007. In vivo quantification of serotonin transporters using [(11)C]DASB and positron emission tomography in humans: modeling considerations. *J Cereb Blood Flow Metab* 27: 205-17

Oquendo MA, Hastings RS, Huang YY, Simpson N, Ogden RT, et al. 2007. Brain serotonin transporter binding in depressed patients with bipolar disorder using positron emission tomography. *Archives of general psychiatry* 64: 201-8

Pacholczyk T, Blakely RD, Amara SG. 1991. Expression cloning of a cocaine- and antidepressant-sensitive human noradrenaline transporter. *Nature* 350: 350-4

Palkovits M, Brownstein M, Saavedra JM. 1974. Serotonin content of the brain stem nuclei in the rat. *Brain research* 80: 237-49

Park SB, Coull JT, McShane RH, Young AH, Sahakian BJ, et al. 1994. Tryptophan depletion in normal volunteers produces selective impairments in learning and memory. *Neuropharmacology* 33: 575-88

Parsey RV, Kegeles LS, Hwang DR, Simpson N, Abi-Dargham A, et al. 2000. In vivo quantification of brain serotonin transporters in humans using [11C]McN 5652. *J Nucl Med* 41: 1465-77

Parsey RV, Kent JM, Oquendo MA, Richards MC, Pratap M, et al. 2006. Acute occupancy of brain serotonin transporter by sertraline as measured by [11C]DASB and positron emission tomography. *Biol Psychiatry* 59: 821-8

Pirker W, Asenbaum S, Hauk M, Kandlhofer S, Tauscher J, et al. 2000. Imaging serotonin and dopamine transporters with 123I-beta-CIT SPECT: binding kinetics and effects of normal aging. *J Nucl Med* 41: 36-44

Popper CW. 1997. Antidepressants in the treatment of attention-deficit/hyperactivity disorder. *The Journal of clinical psychiatry* 58 Suppl 14: 14-29; discussion 30-1

Praschak-Rieder N, Willeit M, Wilson AA, Houle S, Meyer JH. 2008. Seasonal variation in human brain serotonin transporter binding. *Archives of general psychiatry* 65: 1072-8

Prescott DM. 1969. *METHODS IN CELL BIOLOGY*. Elsevier Science.

Rahmim A, Zaidi H. 2008. PET versus SPECT: strengths, limitations and challenges. *Nuclear medicine communications* 29: 193-207

Ramamoorthy S, Bauman AL, Moore KR, Han H, Yang-Feng T, et al. 1993. Antidepressant- and cocaine-sensitive human serotonin transporter: molecular cloning, expression, and chromosomal localization. *Proceedings of the National Academy of Sciences of the United States of America* 90: 2542-6

Reimold M, Batra A, Knobel A, Smolka MN, Zimmer A, et al. 2008. Anxiety is associated with reduced central serotonin transporter availability in unmedicated patients with unipolar major depression: a [11C]DASB PET study. *Mol Psychiatry* 13: 606-13, 557

Reith ME, Li MY, Yan QS. 1997. Extracellular dopamine, norepinephrine, and serotonin in the ventral tegmental area and nucleus accumbens of freely moving rats during intracerebral dialysis following systemic administration of cocaine and other uptake blockers. *Psychopharmacology (Berl)* 134: 309-17

Rocha BA, Goulding EH, O'Dell LE, Mead AN, Coufal NG, et al. 2002. Enhanced locomotor, reinforcing, and neurochemical effects of cocaine in serotonin 5-hydroxytryptamine 2C receptor mutant mice. *The Journal of neuroscience : the official journal of the Society for Neuroscience* 22: 10039-45

Rosel P, Arranz B, Vallejo J, Oros M, Menchon JM, et al. 1997. High affinity [3H]imipramine and [3H]paroxetine binding sites in suicide brains. *J Neural Transm* 104: 921-9

Saudou F, Amara DA, Dierich A, LeMeur M, Ramboz S, et al. 1994. Enhanced aggressive behavior in mice lacking 5-HT1B receptor. *Science* 265: 1875-8

Saulin A, Savli M, Lanzenberger R. 2012. Serotonin and molecular neuroimaging in humans using PET. *Amino Acids* 42: 2039-57

Savli M, Bauer A, Mitterhauser M, Ding YS, Hahn A, et al. 2012. Normative database of the serotonergic system in healthy subjects using multi-tracer PET. *Neuroimage* 63: 447-59

Scatchard G. 1949. THE ATTRACTIONS OF PROTEINS FOR SMALL MOLECULES AND IONS. *Annals of the New York Academy of Sciences* 51: 660-72

Schou M, Halldin C, Sovago J, Pike VW, Hall H, et al. 2004. PET evaluation of novel radiofluorinated reboxetine analogs as norepinephrine transporter probes in the monkey brain. *Synapse* 53: 57-67

Schultz W. 1998. Predictive reward signal of dopamine neurons. *Journal of neurophysiology* 80: 1-27

Schumann CM, Amaral DG. 2006. Stereological Analysis of Amygdala Neuron Number in Autism. *The Journal of Neuroscience* 26: 7674-79

Seeger G, Schloss P, Schmidt MH. 2001. Functional polymorphism within the promotor of the serotonin transporter gene is associated with severe hyperkinetic disorders. *Mol Psychiatry* 6: 235-8

Severson JA, Marcusson JO, Osterburg HH, Finch CE, Winblad B. 1985. Elevated density of [3H]imipramine binding in aged human brain. *Journal of neurochemistry* 45: 1382-9

Shank RP, Vaught JL, Pelley KA, Setler PE, McComsey DF, Maryanoff BE. 1988. McN-5652: a highly potent inhibitor of serotonin uptake. *The Journal of pharmacology and experimental therapeutics* 247: 1032-8

Shen HW, Hagino Y, Kobayashi H, Shinohara-Tanaka K, Ikeda K, et al. 2004. Regional differences in extracellular dopamine and serotonin assessed by in vivo microdialysis in mice lacking dopamine and/or serotonin transporters. *Neuropsychopharmacology : official publication of the American College of Neuropsychopharmacology* 29: 1790-9

Solbach C, Reischl G, Machulla H-J. 2004. Determination of Reaction Parameters for the Synthesis of the Serotonin Transporter Ligand [11C]DASB: Application in a Remote-Controlled High Yield Synthesis. *Radiochim. Acta.*: 341-44

Solich J, Faron-Gorecka A, Kusmider M, Palach P, Gaska M, Dziedzicka-Wasylewska M. 2011. Norepinephrine transporter (NET) knock-out upregulates dopamine and serotonin transporters in the mouse brain. *Neurochemistry international* 59: 185-91

Soret M, Bacharach SL, Buvat I. 2007. Partial-volume effect in PET tumor imaging. *J Nucl Med* 48: 932-45

Staley JK, Basile M, Flynn DD, Mash DC. 1994. Visualizing dopamine and serotonin transporters in the human brain with the potent cocaine analogue [125I]RTI-55: in vitro binding and autoradiographic characterization. *Journal of neurochemistry* 62: 549-56

Staley JK, Sanacora G, Tamagnan G, Maciejewski PK, Malison RT, et al. 2006. Sex differences in diencephalon serotonin transporter availability in major depression. *Biol Psychiatry* 59: 40-7

Stockmeier CA, Shapiro LA, Haycock JW, Thompson PA, Lowy MT. 1996. Quantitative subregional distribution of serotonin1A receptors and serotonin transporters in the human dorsal raphe. *Brain research* 727: 1-12

Suehiro M, Scheffel U, Ravert HT, Dannals RF, Wagner HN, Jr. 1993. [11C](+)McN5652 as a radiotracer for imaging serotonin uptake sites with PET. *Life Sci* 53: 883-92

Swatton JE, Prabakaran S, Karp NA, Lilley KS, Bahn S. 2004. Protein profiling of human postmortem brain using 2-dimensional fluorescence difference gel electrophoresis (2-D DIGE). *Mol Psychiatry* 9: 128-43

Takano A, Varrone A, Gulyas B, Karlsson P, Tauscher J, Halldin C. 2008. Mapping of the norepinephrine transporter in the human brain using PET with (S,S)-[18F]FMeNER-D2. *Neuroimage* 42: 474-82

Tatsumi M, Groshan K, Blakely RD, Richelson E. 1997. Pharmacological profile of antidepressants and related compounds at human monoamine transporters. *European journal of pharmacology* 340: 249-58

Tejani-Butt SM, Ordway GA. 1992. Effect of age on [3H]nisoxetine binding to uptake sites for norepinephrine in the locus coeruleus of humans. *Brain research* 583: 312-5

Tejani-Butt SM, Yang J, Zaffar H. 1993. Norepinephrine transporter sites are decreased in the locus coeruleus in Alzheimer's disease. *Brain research* 631: 147-50

Torres GE, Gainetdinov RR, Caron MG. 2003. Plasma membrane monoamine transporters: structure, regulation and function. *Nature reviews. Neuroscience* 4: 13-25

Tupala E, Hall H, Bergstrom K, Sarkioja T, Rasanen P, et al. 2001. Dopamine D(2)/D(3)-receptor and transporter densities in nucleus accumbens and amygdala of type 1 and 2 alcoholics. *Mol Psychiatry* 6: 261-7

Tzourio-Mazoyer N, Landeau B, Papathanassiou D, Crivello F, Etard O, et al. 2002. Automated anatomical labeling of activations in SPM using a macroscopic anatomical parcellation of the MNI MRI single-subject brain. *Neuroimage* 15: 273-89

Underwood MD, Kassir SA, Bakalian MJ, Galfalvy H, Mann JJ, Arango V. 2012. Neuron density and serotonin receptor binding in prefrontal cortex in suicide. *Int J Neuropsychopharmacol* 15: 435-47

van Dyck CH, Malison RT, Seibyl JP, Laruelle M, Klumpp H, et al. 2000. Age-related decline in central serotonin transporter availability with [(123)I]beta-CIT SPECT. *Neurobiol Aging* 21: 497-501

Varnas K, Halldin C, Hall H. 2004. Autoradiographic distribution of serotonin transporters and receptor subtypes in human brain. *Hum Brain Mapp* 22: 246-60

Vizi ES, Zsilla G, Caron MG, Kiss JP. 2004. Uptake and release of norepinephrine by serotonergic terminals in norepinephrine transporter knock-out mice: implications for the action of selective serotonin reuptake inhibitors. *The Journal of neuroscience : the official journal of the Society for Neuroscience* 24: 7888-94

Way BM, Lacan G, Fairbanks LA, Melega WP. 2007. Architectonic distribution of the serotonin transporter within the orbitofrontal cortex of the vervet monkey. *Neuroscience* 148: 937-48

White KJ, Walline CC, Barker EL. 2005. Serotonin transporters: implications for antidepressant drug development. *The AAPS journal* 7: E421-33

Wilson AA, Ginovart N, Schmidt M, Meyer JH, Threlkeld PG, Houle S. 2000. Novel radiotracers for imaging the serotonin transporter by positron emission tomography: synthesis, radiosynthesis, and in vitro and ex vivo evaluation of (11)C-labeled 2-(phenylthio)araalkylamines. *Journal of medicinal chemistry* 43: 3103-10

Wilson AA, Houle S. 1999. Radiosynthesis of carbon-11 labelled N-methyl-2-(arylthio)benzylamines: potential radiotracers for the serotonin reuptake receptor. *Journal of Labelled Compounds and Radiopharmaceuticals* 42: 1277-88

Xu F, Gainetdinov RR, Wetsel WC, Jones SR, Bohn LM, et al. 2000. Mice lacking the norepinephrine transporter are supersensitive to psychostimulants. *Nature neuroscience* 3: 465-71

Yamamoto M, Suhara T, Okubo Y, Ichimiya T, Sudo Y, et al. 2002. Age-related decline of serotonin transporters in living human brain of healthy males. *Life Sci* 71: 751-7

Yu AJ, Dayan P. 2005. Uncertainty, neuromodulation, and attention. *Neuron* 46: 681-92

Zhou FC, Lesch KP, Murphy DL. 2002. Serotonin uptake into dopamine neurons via dopamine transporters: a compensatory alternative. *Brain research* 942: 109-19

Zhou FM, Liang Y, Salas R, Zhang L, De Biasi M, Dani JA. 2005. Corelease of dopamine and serotonin from striatal dopamine terminals. *Neuron* 46: 65-74